

Strömgren – near-infrared photometry of the Baade’s Window. I. The bulge globular cluster NGC 6528 and the surrounding field.

A. Calamida^{2,3}, G. Bono^{3,4}, E. P. Lagioia⁵, A. P. Milone⁶, M. Fabrizio⁷, I. Saviane⁸, C. Moni Bidin⁹, F. Mauro¹⁰, R. Buonanno⁴, I. Ferraro³, G. Iannicola³, and M. Zoccali¹¹

¹ Based on observations collected with EFOSC2@NTT (Program ID:085.D-0374).

² Space Telescope Science Institute, 3700 San Martin Drive, Baltimore, MD 21218
e-mail: calamida@stsci.edu

³ INAF-Osservatorio Astronomico di Roma, Via Frascati 33, 00040, Monte Porzio Catone, Italy
e-mail: annalisa.calamida@oa-roma.inaf.it; ivan.ferraro@oa-roma.inaf.it; giacinto.iannicola@oa-roma.inaf.it

⁴ Università di Roma Tor Vergata, Via della Ricerca Scientifica 1, 00133 Rome, Italy
e-mail: Giuseppe.Bono@roma2.infn.it; roberto.buonanno@roma2.infn.it

⁵ Dipartimento di Fisica e Astronomia, Università di Bologna, Viale Berti Pichat, 6/2, 40127, Bologna, Italy
e-mail: edoardo.lagioia2@unibo.it

⁶ Research School of Astronomy and Astrophysics, The Australian National University, Cotter Road, Weston, ACT, 2611, Australia
e-mail: milone@mso.anu.edu.au

⁷ INAF-Osservatorio Astronomico di Collurania, Teramo
e-mail: fabrizio@oa-teramo.inaf.it

⁸ ESO Chile, Santiago, Chile
e-mail: isaviane@eso.org

⁹ Instituto de Astronomía, Universidad Católica del Norte, Av. Angamos 0610, Antofagasta, Chile
e-mail: cmoni@ucn.cl

¹⁰ Universidad de Concepción, Concepción, Chile
e-mail: fmauro@astroudec.cl

¹¹ Pontificia Universidad Católica de Chile, Av. Vicuna Mackenna 4860, 782-0436 Macul, Santiago, Chile
e-mail: mzoccali@astro.puc.cl

ABSTRACT

We present Strömgren and near-infrared (NIR) photometry of the bulge cluster NGC 6528 and its surrounding field in the Baade’s Window. *uvby* images have been collected with EFOSC2 on the New Technology Telescope (NTT, La Silla, ESO). The NIR catalogs are based on *J, K*-band VIRCAM@VISTA (Paranal, ESO) and SOFI@NTT photometry. The matching of the aforementioned data sets with Hubble Space Telescope photometry allowed us to obtain proper-motion-cleaned samples of NGC 6528 and bulge stars. Furthermore, we were able to correct the Strömgren–NIR photometry for differential reddening. The huge color sensitivity of the Strömgren–NIR Color–Magnitude–Diagrams (CMDs) helped us in disentangling age and metallicity effects. The red-giant branch (RGB) of NGC 6528 is well reproduced in all the CMDs by adopting scaled-solar isochrones with solar abundance, i.e. $Z = 0.0198$, or α -enhanced isochrones with the same iron content, i.e. $Z = 0.04$, and an age range of $t = 10 - 12$ Gyr. The same isochrones well reproduce most of the color spread of the Baade’s window RGB. These findings support age estimates present in literature for NGC 6528.

We also performed a new theoretical visual–NIR metallicity calibration based on the Strömgren index m_1 and on visual–NIR colors for red-giant (RG) stars. Scaled-solar and α -enhanced models have been adopted and we validated the new Metallicity–Index–Color (MIC) relations by applying them to estimate the photometric metal abundance of a sample of field RGs and of a metal-poor (M 92, $[\text{Fe}/\text{H}] \sim -2.3$) and a metal-rich (NGC 6624, $[\text{Fe}/\text{H}] \sim -0.7$) globular cluster. We applied the calibration to estimate the mean metal abundance of NGC 6528, finding $[\text{Fe}/\text{H}] = [\text{M}/\text{H}] = -0.04 \pm 0.02$, with a mean intrinsic dispersion of $\sigma = 0.27$ dex, by averaging the metallicities obtained with the scaled-solar $[m]$, $y - J$ and $[m]$, $y - K$ MIC relations, and of -0.11 ± 0.01 , with $\sigma = 0.27$ dex, by using the m_1 , $y - J$ and m_1 , $y - K$ relations. These findings would support the results of Zoccali et al. (2004) based on high-resolution spectroscopy, which give $[\text{Fe}/\text{H}] = -0.10 \pm 0.2$ for NGC 6528, and a low α -enhancement of $[\alpha/\text{Fe}] = 0.1$, and of Carretta et al. (2001), that find $[\text{Fe}/\text{H}] = 0.07 \pm 0.01$, with a modest α -enhancement, $[\alpha/\text{Fe}] = 0.2$. By applying the scaled-solar MIC relations to the sample of Baade’s window RGs, we find a metallicity distribution which extend approximately from $[\text{Fe}/\text{H}] \sim -1.0$ up to $[\text{Fe}/\text{H}] \sim 1$ dex, with two metallicity peaks at $[\text{Fe}/\text{H}] \approx -0.2$ and $[\text{Fe}/\text{H}] \approx 0.55$ ($[m]$, $y - J$ and $[m]$, $y - K$ relations), and $[\text{Fe}/\text{H}] \approx -0.25$ and $[\text{Fe}/\text{H}] \approx 0.4$ (m_1 , $y - J$ and m_1 , $y - K$ relations). These findings are in fairly good agreement with the spectroscopic studies of Zoccali et al. (2008), and Hill et al. (2011) for the Baade’s window, of Uttenhaler et al. (2012) for a region centered at $(l, b) = (0^\circ, -10^\circ)$, and with the recent results of the ARGOS surveys for the bulge (Freeman et al. 2013, Ness et al. 2013a).

Key words. stars: abundances — stars: evolution – Galaxy: globular clusters

1. Introduction

The study of the Galactic bulge is fundamental to understand the star formation history of the Galaxy. Moreover, the Milky Way bulge is the closest galaxy bulge that can be observed, and constraining its properties is of great help to the study of more distant galaxies. The Galactic bulge is, indeed, dominated by metal-rich old stars ($t > 10$ Gyr, Zoccali et al. 2003), but the presence of a few intermediate-age stars is not excluded (van Loon et al. 2003; Bensby et al. 2013). The metallicity distribution of red-giant (RG) stars in the bulge spans a range from $[\text{Fe}/\text{H}] \approx -1.5$ to 0.5, according to high-resolution spectroscopy of ~ 800 stars (Hill et al. 2011; Zoccali et al. 2008, hereafter ZO08). Furthermore, Gonzalez et al. (2011) and Uttenthaler et al. (2012) recently showed that bulge stars are α -enhanced when compared with thin disk stars. Moreover, there is evidence that the α enhancement decreases at higher metallicities. More recently, the ARGOS (Abundances and Radial velocity Galactic Origins Survey) survey provided medium-resolution spectroscopy for $\sim 25,000$ red clump stars distributed in 28 two-degree fields at different Galactic longitudes and for latitudes $b = -5, -7.5, -10^\circ$. They found that the bulge stellar content is made by two spatially and chemically distinct sub-populations. *a*) A thin more metal-rich sub-sample, peaking at super-solar iron abundance ($[\text{Fe}/\text{H}] \approx 0.15$), that is kinematically colder and closer to the Galactic plane (A component). This component is associated with the thin disc of the Galaxy. *b*) A thick more metal-poor sub-sample (peaking at $[\text{Fe}/\text{H}] \approx -0.25$) that is uniformly distributed across the selected fields. This component is associated with the boxy/peanut bulge (Ness et al. 2013a). They also identify a main more metal-poor component at $[\text{Fe}/\text{H}] = -0.66$, and two other peaks in their metallicity distribution function (MDF), at $[\text{Fe}/\text{H}] = -1.16$, and -1.73 , that appear to be associated with the thick disk and with the inner halo (Freeman et al. 2013; Ness et al. 2013a). These results are also in agreement with the high-resolution spectroscopy of a sample of 58 micro-lensed bulge dwarfs by Bensby et al. (2013). Their MDF presents three main "bumps" at $[\text{Fe}/\text{H}] \approx -0.7, -0.25$, and 0.3, which are in agreement with the three main populations identified by the ARGOS survey. The above MDFs agree quite well with the results by Hill et al. (2011) for the Baade's window (BW). They found, by using high-resolution spectra for 219 bulge red clump giants, a bi-modal metallicity distribution, with peaks at $[\text{Fe}/\text{H}] \sim -0.3$ and 0.3. The two main components seem to show different kinematical properties, with the most metal-poor stars more compatible with an old-spheroid, while the metal-rich component with a bar population. A double peaked MDF was also found by Uttenthaler et al. (2012), based on medium-resolution spectra of ~ 400 RGs in a bulge field centered at $(l, b) = (0^\circ, -10^\circ)$. The two peaks are located at $[\text{M}/\text{H}] \sim -0.6$ and ~ 0.3 , suggesting that their metal-poor metallicity peak is shifted towards the more metal-poor regime when compared to the metal-poor peaks found by Bensby et al. (2011) and Hill et al. (2011). Moreover, they also found that the metal-rich stars show a smaller velocity dispersion compared to metal-poor stars. On the basis of this evidence they suggest that the metal-rich population, making up $\approx 30\%$ of the sample, could belong to the bar, while the metal-poor one to the Galactic bulge.

A quantitative explanation of how the Galactic bulge formed is still missing, and medium- and high-resolution spectroscopic studies are tracing different regions of the bulge. Some evidence points to constrain the Milky Way bulge as a classical bulge, others favors a pseudo-bulge. The fact that the RR Lyrae do not show evidence of a bar is also suggesting that the truly old (hor-

izontal branch stars) bulge population forms a spherical bulge, while the intermediate-age population (red clump stars) form a boxy/peanut bulge (Vásquez et al. 2013; Dékány et al. 2013).

In this context, an interesting region to constrain the bulge nature, is the BW. It is characterized by a low-reddening, $E(B - V) < 0.6$ mag, and by the presence of two Galactic globular clusters (GGCs), namely NGC 6522 and NGC 6528. The former is classified as a bulge metal-intermediate cluster ($[\text{Fe}/\text{H}] \sim -1.3 / -1.2$ dex). Calamida et al. (2011) estimated a mean metal-abundance of $[\text{Fe}/\text{H}] = -1.0$ for this cluster, by adopting a Strömgren theoretical metallicity calibration based on the hk index. The latter -NGC 6528- is among the most metal-rich GGCs. Recent spectroscopic investigations, based on high-resolution spectra, suggested for this cluster a solar metallicity and a modest α -enhancement. Carretta et al. (2001), by using four red horizontal-branch (RHB) stars, found $[\text{Fe}/\text{H}] = 0.07 \pm 0.01$ and an α -enhancement of $[\alpha/\text{Fe}] \approx 0.2$, while Zoccali et al. (2004), by using three RGB stars found $[\text{Fe}/\text{H}] = 0.1 \pm 0.2$ and $[\alpha/\text{Fe}] = 0.1 \pm 0.1$. More recently Origlia et al. (2005), using high-resolution NIR spectra of four bright giants, found $[\text{Fe}/\text{H}] = 0.17 \pm 0.01$ and a higher α -enhancement, $[\alpha/\text{Fe}] = 0.33 \pm 0.01$. The quoted measurements indicate that NGC 6528 is an ideal laboratory not only to constrain the α -enhancement in old metal-rich systems, but also to shed new light on the possible occurrence of an age-metallicity relation among the most metal-rich Galactic globulars (Rakos & Schombert 2005; Dotter et al. 2011).

The metallicity estimates, based on photometric indices, of field and cluster stars in the bulge are partially hampered by the occurrence of differential reddening across the field of view and by the mix of stellar populations belonging to the bulge, the thick and thin disk and to globulars. The first problem can be partially overcome by using NIR bands, while the latter is more complex. The use of optical-NIR color-color planes, in particular Strömgren-NIR planes, to separate cluster and field stars (Calamida et al. 2009; Bono et al. 2010) is limited by the fact that the metallicity distributions of bulge, thick/thin disk and NGC 6528 all peak around solar chemical composition. Furthermore, the use of the color-color plane to separate field and cluster stars does require precise and deep photometry in at least three optical-NIR bands.

In the current paper we adopt ground-based photometry and use the Strömgren-NIR color-color planes to perform a preliminary selection of bulge, disk and cluster stars. We also take advantage of optical and NIR space photometry collected with Advanced Camera for Surveys (ACS) and Wide Field Camera 3 (WFC3) on board the Hubble Space Telescope (HST) to estimate proper motions and further select the different stellar components. The ground-based Strömgren-NIR photometry is then adopted to estimate the metallicity distribution of bulge and cluster RGs, by applying a new theoretical calibration of the Strömgren $m_1 = (v - b) - (b - y)$ metallicity index, based on visual-NIR colors.

This is the first paper of a series devoted to Strömgren-NIR photometry of metal-rich GGCs. In this initial investigation, we derive and test a new theoretical calibration of the m_1 index, based on visual-NIR colors for RG stars. The new calibration is adopted to constrain the metallicity distribution of NGC 6528 and its surrounding field.

We favored the adoption of the visual-NIR colors to derive Metallicity-Index-Color (MIC) relations, since they have two clear advantages when compared with indices only based on Strömgren colors. *a*) They are not hampered by the presence of CN, CH , and NH molecular absorption bands. Two strong CN

bands ($\lambda = 4142$ and $\lambda = 4215$ Å) affects the v filter, while the strong CH -band at $\lambda = 4300$ Å might affect both the v and the b , and the NH -band at $\lambda = 3360$ Å plus the two CN bands at $\lambda = 3590$ and $\lambda = 3883$ Å might affect the u ; *ib*) They have a stronger sensitivity to effective temperature. The quoted molecular bands still affect the the new visual–NIR MIC relations, but only through the Strömgren m_1 index.

The new MIC relations are based on scaled-solar and α -enhanced evolutionary models. The adopted evolutionary models were transformed into the observational plane by adopting bolometric corrections and color–temperature transformations based on atmosphere models constructed by adopting the same chemical mixtures. They are valid in the metallicity range $-2.5 < [\text{Fe}/\text{H}] < 0.5$. The new MIC relations were validated by estimating the abundances of GGCs, from the very metal-poor M 92 ($[\text{Fe}/\text{H}] \sim -2.3$) to the bulge metal-rich cluster NGC 6624 ($[\text{Fe}/\text{H}] \sim -0.6$), and of field RG stars, and by comparing them with medium- and high-resolution spectroscopic measurements.

The structure of the current paper is as follows. In §2 we discuss in detail the observations and data reduction, while in §3 we describe the photometric calibration. In §4 we present the Strömgren–NIR catalogs adopted in this paper. Section 5 deals with the approach adopted to calibrate the visual–NIR MIC relations for giant stars, while in §6 we present the different tests we performed to validate the current theoretical MIC relations together with the comparison between photometric estimates and spectroscopic measurements of metal abundances. In §7 we study the metallicity distribution of NGC 6528 and the Baade’s window RGs. The summary of the results and a brief discussion concerning further developments of the new MIC relations are given in §8.

2. Observations and data reduction

We adopt Strömgren photometry of the bulge cluster NGC 6528 collected with the EFOSC2 camera on the NTT in 2010 (Program ID: 085.D-0374). The CCD is a Loral/Lesser Thinned AR coated 2048×2048 chip, with a pixel size of $15 \mu\text{m}$, corresponding to a pixel scale of $0''.12$. The field of view (FoV) is thus $4.1' \times 4.1'$. We used the normal read-out mode and the 2×2 binning, getting an effective pixel scale of $0''.24$.

We collected $2u$ -, $2v$ -, $3b$ - and $3y$ -band images during two different nights (July 11 and 13), with exposure times ranging from 60 to 2,500s and seeing from $0''.7$ to $1''.0$. The total FoV is $\approx 5' \times 5'$ and includes the cluster center. The footprints of the observed fields are shown in Fig. 1 (blue), while the log of the observations is given in Table 1.

Halo

clusters for which we have published Strömgren photometry (Grundahl et al. 2000; Grundahl, Stetson, & Andersen 2002; Calamida et al. 2007, hereafter CA07) were observed during the same nights with similar airmass conditions. The purpose was to adopt cluster stars as a set of standards to derive calibration curves for the observing nights. These will then be applied to calibrate the photometry of bulge clusters observed soon after or before the calibrating clusters. In order to calibrate the photometry of NGC 6528 we observed NGC 6752 during the same nights, collecting $6u$ -, $6v$ -, $6b$ - and $6y$ -band images for a total FoV of $\approx 4' \times 4'$ centered on the cluster. These observations overlap with the FoV of our published photometry for NGC 6752, that will be later adopted to calibrate the data set. The log of NGC 6752 observations is also shown in Table 1.

Raw images were pre-processed by using tasks available in the IRAF data analysis environment for bias subtraction and flat-

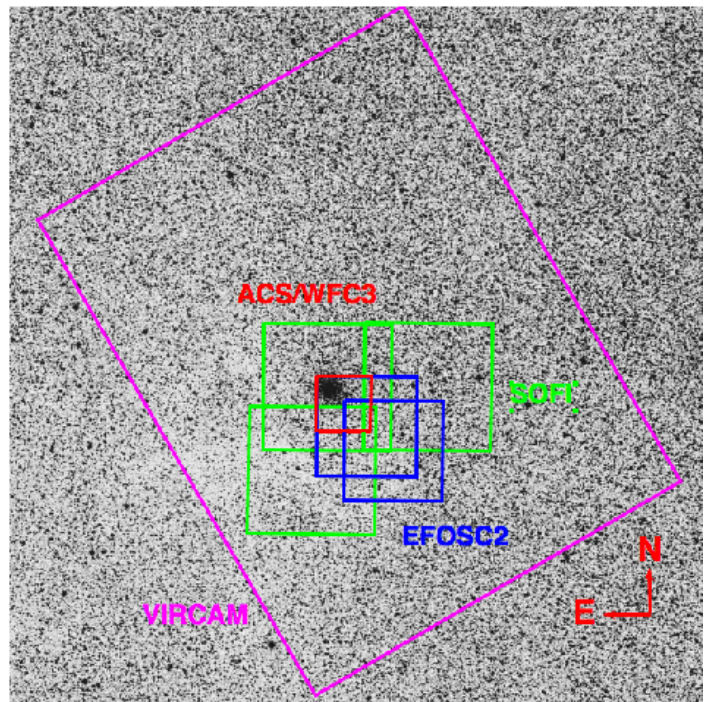


Fig. 1. Footprints of the different optical – NIR data sets adopted in the study of the bulge cluster NGC 6528 and its surrounding field.

fielding. To flat-field these data we adopted median sky flats collected during the three observing nights. The photometry was performed using DAOPHOT IV/ALLSTAR and ALLFRAME (Stetson 1987, 1991, 1994). We first estimated an analytical point-spread function (PSF) for each frame by selecting bright, isolated stars, uniformly distributed on the chip. A Moffat analytical function quadratically variable on the chip was assumed for the PSF. We performed PSF analytical photometry on each image with the task ALLSTAR. In order to obtain a global star catalog for each cluster and each night, we used the task DAOMATCH/DAOMASTER (Stetson 1994) and then performed simultaneous PSF-fitting photometry with the task ALLFRAME. The final star catalogs of the two nights of observations of NGC 6528 include $\approx 22,000$ (July 11) and $\approx 10,000$ stars (July 13), with a measure in at least two bands.

The NIR photometry of NGC 6528 is from SOFI (Son of ISAAC) on NTT and VIRCAM on VISTA (Visible and Infrared Survey Telescope for Astronomy, Paranal, ESO). The SOFI data set consists of 111 J -, 12 H - and 111 K_s -band images (see the green footprints in Fig. 1). The images were pre-reduced with a specific IRAF task pipeline kindly provided by M. Dall’Ora. As for EFOSC2, the photometry of the SOFI images was carried out with DAOPHOT IV/ALLSTAR. A single list of improved positions and instrumental magnitudes for the stars located in overlapping fields was obtained by using DAOMATCH/DAOMASTER.

The VISTA Variables in the Vía Láctea (VVV) Survey (Minniti et al. 2010; Catelan et al. 2011) is one of six ESO Public Surveys operating on VISTA, scanning the Galactic bulge ($-10 \leq l \leq +10$, $-10 \leq b \leq +5$) and the adjacent part of the southern disk ($-65 \leq l \leq -10$, $-2 \leq b \leq +2$). The survey collects data in five NIR bands ($YZJHK_s$) with the VIRCAM camera (Emerson et al. 2010), an array of sixteen 2048×2048 pixel detectors with a pixel scale of $0''.341$. VVV images extend several magnitudes fainter than the Two Micron All Sky Survey

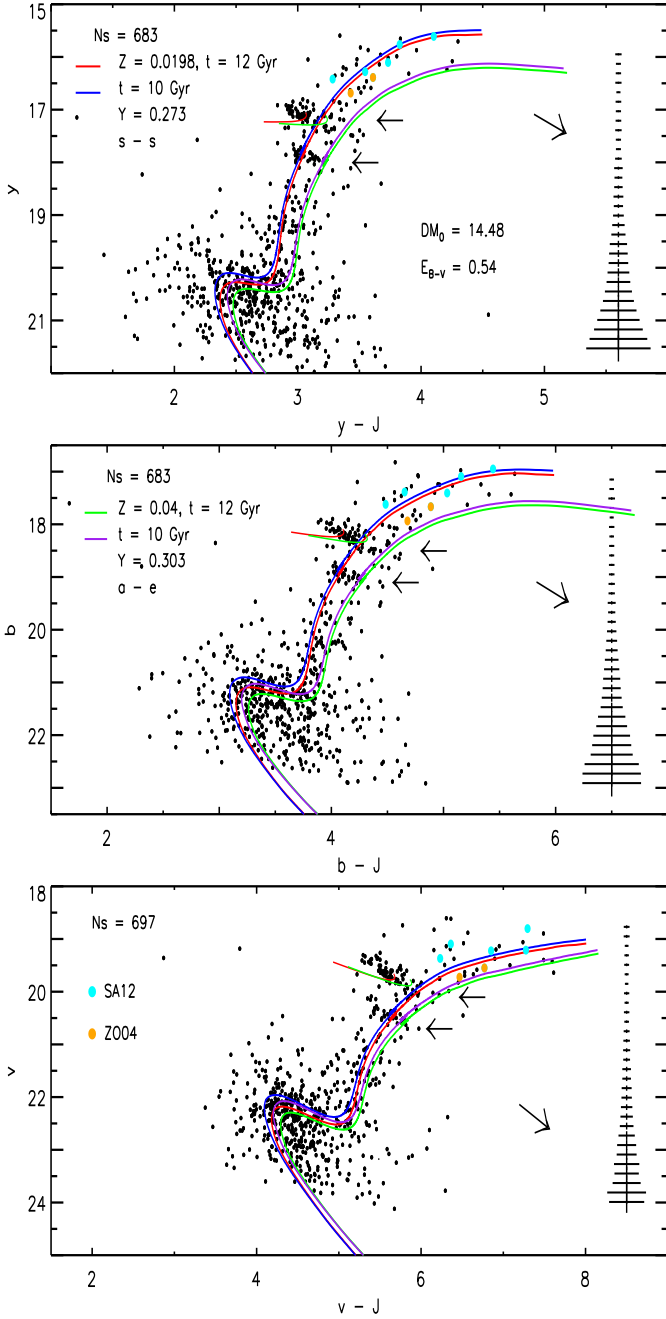


Fig. 2. y , $y - J$ (top), b , $b - J$ (middle), v , $v - J$ (bottom) CMDs of NGC 6528. Stars have been selected according to proper motions and photometric accuracy and corrected for differential reddening. The red and green lines display cluster isochrones at fixed age but different chemical compositions. The blue and the purple lines display younger isochrones for the same chemical compositions (see labeled values). The adopted true distance modulus and mean reddening are labeled. The cluster isochrones are based on evolutionary models computed by assuming either a scaled-solar (s-s, red and blue) and an α -enhanced (α -e) chemical mixture (green and purple). Orange and cyan filled dots mark RGs with spectroscopic abundances from Z004 and SA12, respectively. The two horizontal arrows mark the location of the RHB (brighter) and of the RGB bump (fainter), while the right bended arrow shows the reddening vector.

(2MASS, Skrutskie et al. 2006), and enjoy increased spatial resolution (Saito et al. 2012). Both of these factors are particularly important for mitigating contaminated photometry in crowded regions such as the cores of globular clusters. We retrieved from the Vista Science Archive website¹ VVV images containing NGC 6528 for a total FoV of $17' \times 22'$ (see purple footprint in

Fig. 1). We also retrieved data for NGC 6624, a cluster adopted later to test the validity of metallicity calibrations. Data were pre-reduced at the Cambridge Astronomical Survey Unit (CASU)² with the VIRCAM pipeline (Irwin et al. 2004). We then performed PSF-fitting photometry by using the VVV-SkZ_pipeline code (Mauro et al. 2013) on the single 2048×2048 pixel chips

¹ <http://horus.roe.ac.uk/vsa/>

² <http://casu.ast.cam.ac.uk/>

extracted from the stacked VVV pawprints (Saito et al. 2012). A quadratically variable Moffat function with $\beta = 3.5$ has been adopted in this case to perform the PSF-fitting photometry on the VIRCAM images.

3. Photometric calibration

3.1. EFOSC2 data set

We first applied aperture corrections to the single cluster instrumental photometric catalogs. The corrections were estimated for the adopted reference y, b, v, u -band images and then applied to the mean magnitudes. Photometry was also corrected according to the exposure times and airmass values of the reference images by adopting the standard La Silla extinction coefficients for the Strömgren filters.

The two corrected instrumental catalogs of NGC 6752 for the nights July 11 and 13 were cross-correlated with the calibrated Strömgren catalog for this cluster. We ended up with a sample of $\approx 5,000$ and $\approx 1,500$ stars in common for the two nights, respectively, to estimate the calibration curves. The stars were selected in photometric accuracy, $\sigma_{y,b,v,u} < 0.1$ mag, and the cluster center was excluded by keeping stars with a distance from the cluster center larger than $1.5'$. The derived calibration curves for the two nights are:

July 11:

$$u = u_i - 1.911(\pm 0.022) + 0.127(\pm 0.010) \times (u_i - b_i),$$

$$v = v_i - 0.907(\pm 0.005),$$

$$b = b_i - 1.215(\pm 0.005) + 0.055(\pm 0.0011) \times (b_i - y_i),$$

$$y = y_i - 1.347(\pm 0.004) + 0.070(\pm 0.009) \times (b_i - y_i)$$

July 13:

$$u = u_i - 1.966(\pm 0.012) + 0.063(\pm 0.006) \times (u_i - b_i),$$

$$v = v_i - 0.993(\pm 0.005),$$

$$b = b_i - 1.240(\pm 0.005) + 0.034(\pm 0.0012) \times (b_i - y_i),$$

$$y = y_i - 1.388(\pm 0.005) + 0.043(\pm 0.012) \times (b_i - y_i)$$

where i stands for *instrumental* magnitude.

We applied these calibration curves to NGC 6528 corrected instrumental photometry for the nights of July 11 and 13. We then merged the two data sets obtaining a final calibrated catalog of 22,986 stars.

The typical accuracy of the absolute zero-point calibration is ~ 0.06 mag for the u -band data and ~ 0.05 mag for the v, b, y -band data.

3.2. SOFI and VIRCAM data sets

The NIR broad-band filters J, H, K_S , with which the SOFI images were collected, have passbands very similar to those used for the observations of the 2MASS survey (Cutri et al. 2003). Therefore, after the aperture corrections were computed for the PSF stars in each single frame by using DAOGROW (Stetson 1990), the instrumental magnitudes were calibrated to the 2MASS system using a set of local standards. The solutions

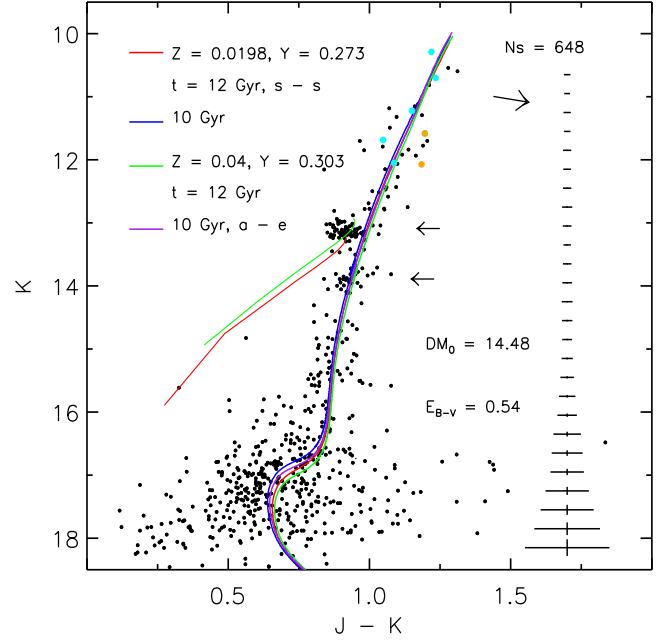


Fig. 3. $K, J - K$ CMD of NGC 6528. Stars have been selected according to proper motions and photometric accuracy and corrected for differential reddening. Symbols and lines are the same as in Fig. 2.

of the calibration equations were found with CCDSTD (Stetson 1993). We ended up with a catalog of $\sim 65,000$ stars, with at least one measurement in two bands. The photometric catalog ranges from the tip of the RGB down to $\sim 0.5 - 1$ mag below the Main Sequence Turn-Off (MSTO).

The VIRCAM photometric catalog was also tied to the 2MASS system. The calibration consisted in applying the classical correction for the zero point and color terms to the ALLFRAME output. The procedure has already been described by Moni Bidin et al. (2011); Chene et al. (2012); Mauro et al. (2013). The use of the VVV-SkZ_pipeline was fundamental for this work, since it is the only photometric procedure for VVV data that manages to provide accurate photometry even for partially saturated stars. The H_{2MASS} -band photometry (hereafter $H_{2MASS} = H, J_{2MASS} = J, K_{S2MASS} = K$) was neglected, since the precision in this filter was not good enough at the limiting magnitudes we are dealing with.

The SOFI and VIRCAM catalogs were matched and we estimated the weighted mean of J and K -band magnitudes. The final merged NIR catalog includes $\approx 50,000$ stars, with an accuracy of ≈ 0.05 mag at $J \approx 19$ mag, and covering a FoV of $\approx 8' \times 8'$.

4. Strömgren–NIR photometry

4.1. NGC 6528

The Strömgren photometry of NGC 6528 was cross-correlated with the NIR photometry and we ended up with a Strömgren–NIR catalog of 22,025 stars. This catalog was then matched to optical and NIR photometry collected with ACS@HST and WFC3@HST (Program IDs: GO9453, GO11664). The reader is referred to LA14 for details on this data set observations and reduction techniques. The final merged catalog includes 3,189 stars and covers a FoV of $\approx 2.2' \times 2.2'$, with the cluster center located in the North-East corner (see red footprint in Fig. 1). We

corrected the photometry for differential extinction by adopting the individual reddening values estimated for each star in the field by LA14.

We then adopted the proper-motion selection of LA14 to obtain a clean sample of 737 cluster stars with a measurement in at least two Strömgren and two NIR bands. The matched catalog reaches 1 mag below the turn-off (TO) with an accuracy of ≈ 0.2 mag at $y \approx 21.5$ mag.

We also matched current NGC 6528 photometry with the high-resolution spectroscopic targets by Zoccali et al. (2004, hereafter Z004, Z008) and Origlia et al. (2005), and *CaT* spectroscopy by Saviane et al. (2012, hereafter SA12). The three RGs in the Z004 sample are located inside our FoV, namely OGLE 357459, OGLE 357480 and I 42, while only one out of the four RGs in the Origlia et al. sample (star 3167), is covered by our catalog. Star OGLE 357480 has a color systematically bluer than cluster RGs and it does not belong to NGC 6528 according to our proper-motion selection; the same outcome applies to star 3167. We ignored both of them. Six stars of SA12 sample were found in common with our Strömgren–NIR photometry. One star, R1-42, is star I 42 of Z004 sample, and the other five, R2-8, R2-41, 1_3704, 1_1044 and 1_2735, belong to NGC 6528 according to current proper-motion selection. We ended up with seven candidate cluster member RGs with spectroscopic abundance measurements available.

Fig. 2 shows the y , $y - J$, b , $b - J$, and v , $v - J$ proper-motion cleaned color-magnitude diagram (CMD) of NGC 6528. Stars have been selected according to the “separation index”³, by keeping the best 90% of the stars for each 0.18 magnitude bin in the ranges $15.5 < y < 22$, $16.7 < b < 23.1$ and $18.5 < v < 24.3$ mag. We excluded the u -band since the photometry is based on only one image per night and it is not accurate enough for this study.

In this analysis, we adopt three different CMDs since, from the empirical point of view, different Strömgren–NIR bands have different photometric accuracy. Moreover, from the theoretical point of view, the Color–Temperature Relations (CTRs) adopted to transform isochrones into the observational plane need to be tested. This is the first time, indeed, that these models are adopted to fit the entire magnitude range from the MS to the RGB in Strömgren–NIR CMDs.

The solid lines in Fig. 2 show isochrones for different ages and different chemical composition, namely $Z = 0.0198$, $Y = 0.273$, scaled-solar, $t = 12$ (red solid line) and $t = 10$ Gyr (blue), and $Z = 0.04$, $Y = 0.303$, α -enhanced ($[\alpha/\text{Fe}] = 0.4$), $t = 12$ (green) and $t = 10$ Gyr (purple). The corresponding scaled-solar and α -enhanced Zero Age Horizontal Branches (ZAHBs, red and green solid lines) for $Z = 0.0198$ and $Z = 0.04$ are also plotted. The adopted chemical compositions have the same iron content, $[\text{Fe}/\text{H}] \sim 0.06$, but different helium and α -element abundances. Isochrones and ZAHBs are from the BASTI data base (Pietrinferni et al. 2004, 2006, hereafter PI06) and evolutionary prescriptions were transformed into the observational plane by using atmosphere models computed assuming scaled-solar and α -enhanced chemical mixtures. We adopt a true distance modulus of $DM_0 = 14.50$ mag (LA14), and a mean reddening of $E(B - V) = 0.54$ mag for NGC 6528. The reddening was estimated as a weighted mean of the values given by the extinction map of Gonzalez et al. (2011) for this FoV and by adopting a standard reddening law, $R_V = A_V/E(B - V) = 3.1$. The extinction coefficients are then estimated by applying the Cardelli et al.

³ The “separation index” quantifies the degree of crowding of a star after PSF photometry has been performed (Stetson et al. 2003).

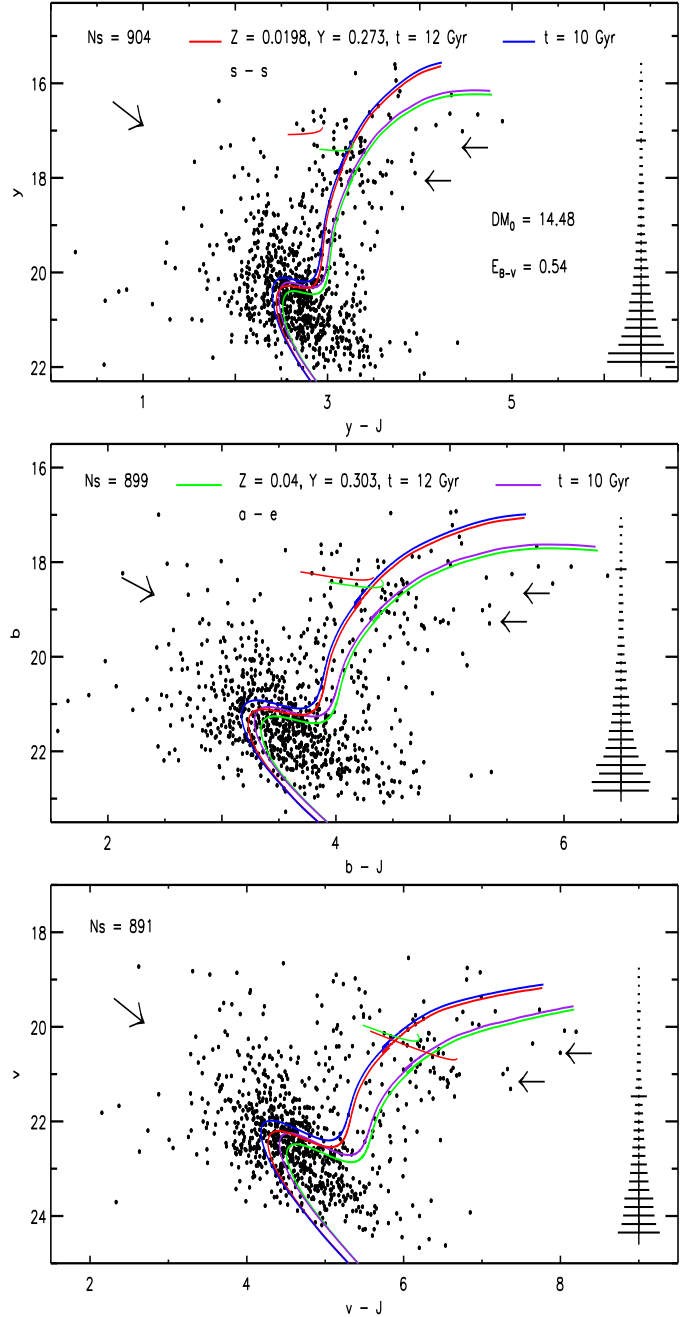


Fig. 4. Same as Fig. 2 but for the field surrounding NGC 6528. Symbols and lines are the same as in Fig. 2.

(1989) reddening relations, finding $A_y = A_V$, $A_b = 1.225 \times A_V$, $A_v = 1.424 \times A_V$, and $E(y - J) = 2.23 \times E(B - V)$ mag, $E(b - J) = 2.91 \times E(B - V)$ mag, and $E(v - J) = 3.527 \times E(B - V)$ mag.

Data plotted in Fig. 2 show a clean sample of NGC 6528 member stars corrected for differential reddening down to 1 mag below the TO. Unfortunately the precision of both Strömgren and NIR photometry (see the error bars in Fig. 2), and the residual uncorrected reddening, do not allow us to properly identify the cluster MSTO. However, evolved evolutionary features can be easily identified in the three CMDs. The RGB bump is identified as an over-density at $y \sim 17.8$ and $y - J \sim 3$ mag, $b \sim 17.8$ and $b - J \sim 4$ mag and $v \sim 20.5$ and $v - J \sim 5.7$ mag (see the arrows in Fig. 2). The RHB is well separated

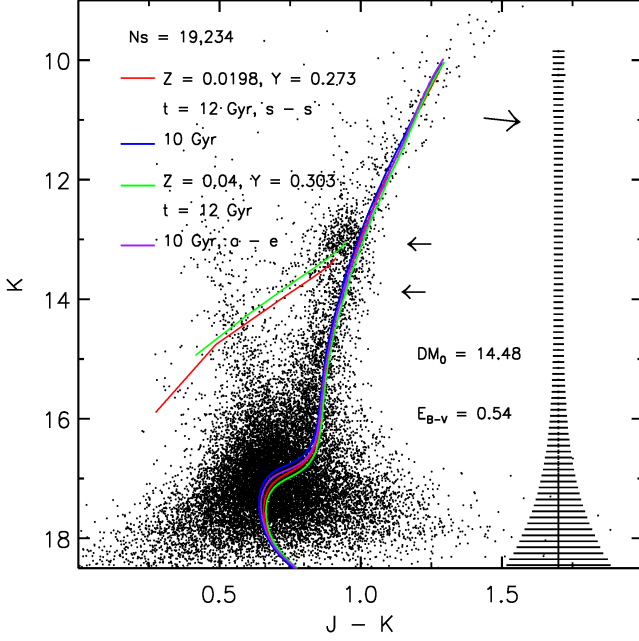


Fig. 5. Same as Fig. 3, but for the field surrounding NGC 6528. Stars have been selected according to photometric accuracy. Cluster isochrones and ZAHBs are plotted by adopting the same distance modulus and reddening. From top to bottom the arrows mark the direction of the reddening vector, the location of the RHB-RC and the RGB bump.

from the RGB and is located at $y \sim 17$ and $y - J \sim 3$, $b \sim 18$ and $b - J \sim 4$ mag and $v \sim 19.5$ and $v - J \sim 5.5$ mag (see the arrows). The scaled-solar models (red and blue solid lines) fit quite well the observations, within the uncertainties, and suggest for this cluster an age of 11 ± 1 Gyr. Interestingly enough, stars from the spectroscopic samples agree quite well with scaled-solar isochrones in the three CMDs. The α -enhanced isochrones (green and purple) attain, as expected, systematically redder colors in the three CMDs. However, the difference in color and in magnitude between the two different sets does not allow us to reach firm conclusions concerning the cluster α -enhancement. Although, the observed RGB-bump stars appear to be systematically bluer than predicted by the α -enhanced isochrones.

We plotted the same candidate cluster stars in the NIR K , $J - K$ CMD in Fig. 3. In this plane the RHB and the RGB-bump are much better defined (see arrows). The same isochrones and ZAHBs of Fig. 2 are over-plotted by adopting the same reddening and distance modulus. It is worth noticing how the isochrones overlap along the MS and the RGB phases in the K , $J - K$ CMD, while, at fixed iron abundance, the α -enhanced models are redder than the scaled-solar models in the Strömgren–NIR CMDs (see Fig. 2). Fig. 3 shows that α -enhanced and scaled-solar isochrones agree quite well, within the uncertainties (see error bars in the figure), with NIR observations, confirming an age of 11 ± 1 Gyr for the cluster. This result is in very good agreement with the age derived by Feltzing & Johnson (2002) for NGC 6528, i.e. 11 ± 2 Gyr. They adopted $F555W$, $F814W$ WFPC2 photometry and astrometry to obtain a proper-motion cleaned CMD for the cluster. To fit the optical CMD they use α -enhanced isochrones by Salasnich et al. (2000) for $Z = 0.04$, a distance modulus of $DM_0 = 14.29$ mag and reddening $E(B - V) = 0.54$ mag.

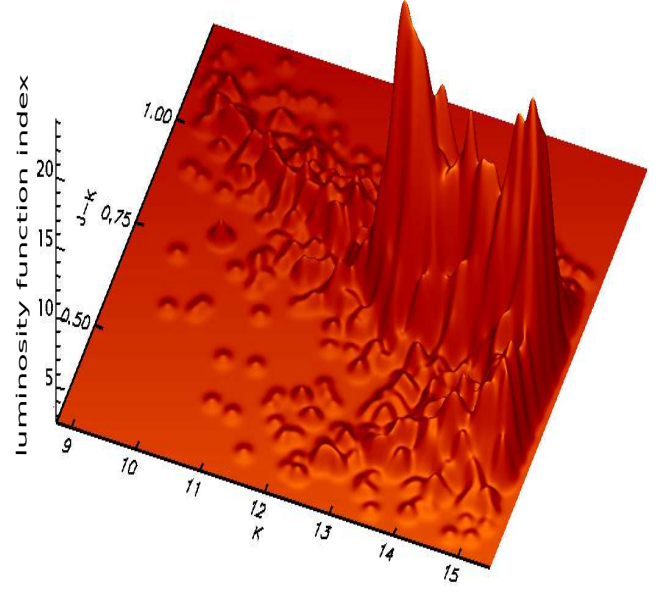


Fig. 6. 3D K , $J - K$ CMD of field stars surrounding NGC 6528, based on VIRCAM-SOFI photometry. The CMD is slightly rotated to better show the separation between blue MS and RG stars. At $K = 14$, MS stars cluster around $J - K = 0.6$, while RGs around $J - K = 0.8$ mag.

Moreover, current estimates are also in fairly good agreement with the results of Momany et al. (2003). They presented NIR photometry of NGC 6528 based on SOFI data - that are included in our data set - and cluster members were selected by adopting HST proper motions. They estimated a cluster age of 12.6 Gyr, by adopting Bertelli et al. (1994) scaled-solar isochrones for $Z = 0.02$ and a distance modulus $DM_0 = 14.44$ mag and $E(B - V) = 0.55$ mag. Finally, our age estimate is in very good agreement with the results of LA14 that find $t = 11 \pm 1$ Gyr, by fitting their optical HST CMD with a scaled-solar isochrone with $[\text{Fe}/\text{H}] = 0.20$ (Dell’Omodarme et al. 2012), and by adopting $DM_0 = 14.50$ mag and $E(B - V) = 0.56$ mag.

4.2. The field surrounding NGC 6528

A clean proper-motion sample of 986 candidate bulge stars is selected from the Strömgren–NIR catalog and plotted on the y , $y - J$, b , $b - J$, and v , $v - J$ CMDs in Fig. 4. In the comparison between theory and observations we adopted the same theoretical framework, reddening and absolute distance modulus as for NGC 6528. Fig. 4 shows that we do not have enough statistics to properly characterize the bulge stellar populations in the Baade’s window. However, data plotted in the the Strömgren–NIR CMDs bring forward a few interesting features:

a) The RGB shows a clear dispersion in color in all the CMDs, mostly given by the presence of both a metallicity and an age spread. Indeed, the adopted isochrones do not bracket the color dispersion along the RGB. Together with the above intrinsic properties the color dispersion is also caused by the effect of residual uncorrected differential reddening (see the arrows in Fig. 4 for the reddening direction), by depth effects and by pho-

tometric errors. Current data set does not allow us to disentangle the above degeneracies.

b) The RHB is not a well defined sequence and red clump (RC) stars are overlapping the RGB.

c) The RGB-bump is not clearly visible, except for a small overdensity of stars ranging from $19.5 \lesssim \nu \lesssim 21$ mag and $5 \lesssim \nu - J \lesssim 6.5$ mag in the $\nu, \nu - J$ CMD.

d) There is a small residual contamination by disk stars located in a sequence brighter and bluer than the MSTO in all the CMDs.

Data plotted in Fig. 4 show that a fraction of observed stars along the MS and the RGB are systematically redder and/or fainter than predicted by adopted cluster isochrones. This result would suggest the possible occurrence of large samples of super metal-rich stars, $[\text{Fe}/\text{H}] > 0.1$, in the Baade’s window. However, these objects could also be explained with an increase either in the mean reddening or in depth or both.

4.3. The RC-RHB stars and the RGB-bump

To shed new light in this interesting open problem, we plotted the entire selected VIRCAM-SOFI catalog in the $K, J - K$ CMD in Fig. 5. The RC-RHB region and the RGB-bump are much better defined compared to Fig. 4 due to the increased statistics and to the reduced sensitivity of NIR colors to effective temperature when compared to optical–NIR colors. The same isochrones of Fig. 4 are over-plotted by adopting the same reddening and distance modulus. This figure shows that the adopted isochrones also agree well with the NIR observations of the bulge stars in the Baade’s window. In particular, the dispersion in color of the bulge MS is quite similar to the dispersion in color of the NGC 6528 CMD at the same magnitude level (see Fig. 3). This suggests that the spread in color is mainly due to photometric errors and residual differential reddening.

However, data plotted in this figure show that the ZAHBs attain a K -band magnitude that is systematically fainter than observed RHB-RC stars. This is an interesting empirical evidence. Indeed, current spectroscopic targets use as stellar tracers RC stars. The selection is performed using NIR CMDs and the region in color and in magnitude they adopt includes not only truly RHB (old [$t > 10$ Gyr], low-mass), but also truly RC (intermediate-age [$t < 8$ Gyr], intermediate-mass) stars. Note that the above separation is far from being an academic debate and, indeed, according to current evolutionary prescriptions, in the former group the central helium-burning takes place in a more massive, electron-degenerate core, while in the latter takes place in a less massive, partially electron-degenerate core (Fiorentino et al. 2012; Coppola et al. 2013).

The above scenario does imply a difference in mean magnitude between the two groups, since RHB stars are in optical and in NIR magnitudes fainter and bluer than RC stars. To further constrain this effect we adopted the entire sample of VIRCAM-SOFI measurements to study the magnitude and color distribution of stars in the RHB-RC region. To avoid NGC 6528 we selected only stars with a distance from the cluster center larger than $\approx 2.5'$. Fig. 6 shows the 3D $K, J - K$ CMD of candidate stars brighter than $K = 15.5$ mag. To select only RGs we then performed a color selection by excluding all stars bluer than $J - K = 0.7$ mag. Fig. 7 (top panel) shows the 2D luminosity function of selected RGs. Central helium burning stars (RC, RHB) display a double peak in the magnitude range $12.5 < K < 13.5$ mag (red and blue arrows, respectively), while the RGB-bump shows a well defined peak at $K = 13.90 \pm 0.05$ mag (green arrow). The middle panel of the same figure shows the projected K -band lu-

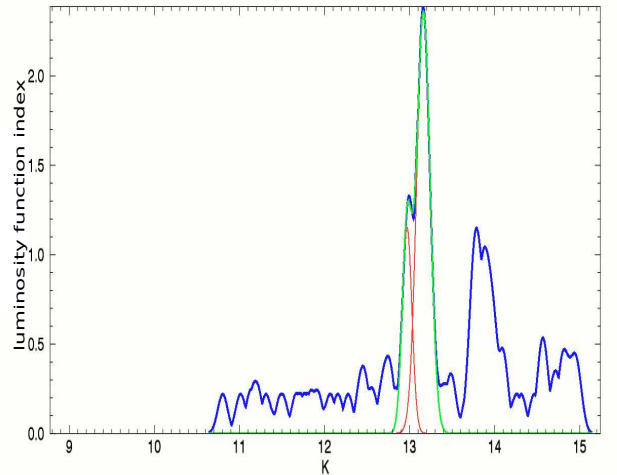
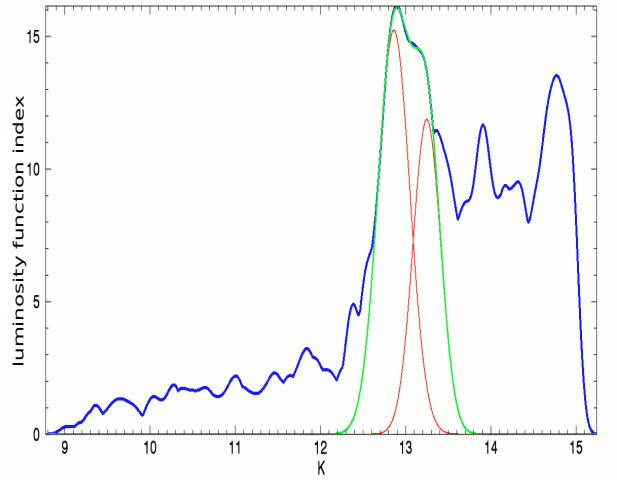
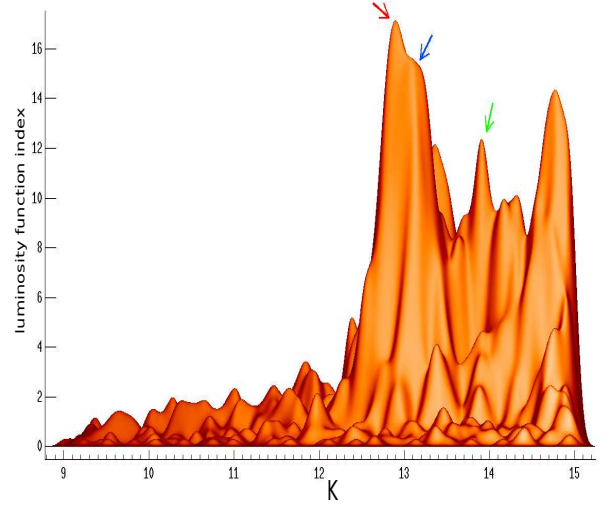


Fig. 7. Top: 2D K -band – based on VIRCAM-SOFI photometry – luminosity function of field RGs surrounding NGC 6528. Middle: Projected K -band luminosity function of field RGs. The two Gaussian functions adopted to fit the RC-RHB regions are over-plotted as red solid lines. The green line shows the cumulative fit. Bottom: Projected K -band luminosity function of NGC 6528 RGs selected according to proper motions. Symbols and lines are the same as in the middle panel.

minosity function of selected RG stars (blue solid line). We fit the RC-RHB region by using two Gaussian functions (red lines), finding the following peaks: $K = 12.86 \pm 0.02$ mag ($\sigma = 0.19$ mag), and $K = 13.25 \pm 0.02$ mag ($\sigma = 0.16$ mag). It is noteworthy that the fainter peak is also systematically bluer ($J - K \approx 0.9$ mag) than the brighter one ($J - K \approx 1.0$ mag, see Fig. 6). This suggests a clear separation both in magnitude and in color between the two peaks.

The bottom panel of Fig. 7 shows the same projected K -band luminosity function of bright ($K \gtrsim 15.5$ mag) proper-motion selected RGs in NGC 6528. The RHB peaks at $K \approx 13.15$ mag, while the RGB-bump at $K = 13.85 \pm 0.05$ mag. The RGB-bump magnitude is in very good agreement with the bump luminosity found by Momany et al. (2003), $K = 13.85 \pm 0.05$ mag, and by Ferraro et al. (2000), $K \approx 13.80$ mag. We then performed a fit of the RHB region by adopting two Gaussian functions (red lines) with peaks at $K = 13.16 \pm 0.02$ mag ($\sigma = 0.08$ mag) and $K = 12.97 \pm 0.02$ mag ($\sigma = 0.06$). The presence of the secondary brighter peak among cluster RGs might be due to minor residual contamination by field stars. Moreover, the faintest peak at $K = 13.16 \pm 0.02$ mag is in very good agreement with $K = 13.20 \pm 0.05$ mag found by Momany et al. (2003) for the RHB of NGC 6528.

The above findings indicate that the fainter peak of field RG luminosity function at $K = 13.25$ mag might be associated with the RHB of the old stellar population, while the brighter peak at $K = 12.86$ mag to RC stars. Interestingly enough, the difference in magnitude between the RC and the RHB peak ($\Delta K \sim 0.4$ mag) supports recent findings concerning the boxy/peanuts shape of the Galactic bulge (McWilliam & Zoccali 2010; Saito et al. 2011).

5. Calibration of new visual–NIR metallicity indices for giant stars

The calibration of Strömgren photometric indices to obtain stellar metal abundances is not a new technique. Empirical calibrations based on such a method have been given by Strömgren (1964); Bond (1970); Crawford (1975); Nissen (1981).

All the derived relations to estimate the metal abundance of RG stars are hampered by the presence of molecular CN , CH and NH -bands that affect the Strömgren uvb filters, and in turn the global metallicity estimates. Moreover, most of the relations presented in literature include the c_1 index, that is based on the u filter. Observations in the u filter are very demanding concerning the telescope time and the photometry in this band is less accurate due to the reduced CCD sensitivity in this wavelength region. For more information about the Strömgren photometric system and metallicity calibration see Calamida et al. (2007, 2012).

In Calamida et al. (2012) we derived, for the first time, a theoretical calibration of a metallicity diagnostic based on the m_1 index and on visual–NIR colors for dwarf stars. We provide in this paper a similar theoretical calibration based on the same colors but for RG stars.

Independent MIC relations were derived using cluster isochrones based on both scaled-solar and α -enhanced ($[\alpha/Fe] = 0.4$) evolutionary models (PI06). Theoretical predictions were transformed into the observational plane by adopting bolometric corrections (BCs) and CTRs based on atmosphere models computed assuming the same heavy element abundances (PI06, Castelli & Kurucz 2006). The Vega flux adopted is from

Castelli & Kurucz (1994)⁴. The metallicities used for the calibration of the MIC relations are: $Z = 0.0001, 0.0003, 0.0006, 0.001, 0.002, 0.004, 0.01, 0.02$ and 0.03 . The adopted Z values indicate the global abundance of heavy elements in the chemical mixture, with a solar metal abundance of $(Z/X)_\odot = 0.0245$. The corresponding iron content for the α -enhanced models can be obtained by using the relationship given by Salaris et al. (1993): $[Fe/H] = [M/H] - \log(0.638f + 0.362)$, where $\log(f) = [\alpha/Fe]$.

Fig. 8 shows nine scaled-solar isochrones plotted in different visual–NIR (left) and Strömgren (right) MIC planes. The J, H, K filters were transformed into the 2MASS photometric system by applying the color transformations by Carpenter et al. (2001). Panels a), b) and c) display the m_1 index versus three visual–NIR colors ($y - K, y - H, y - J$), while the panels d), e) and f) the m_1 index versus three Strömgren colors ($u - y, v - y, b - y$). The evolutionary phases plotted in this figure range from approximately the base (open square) to the tip of the RGB (asterisk).

The two different sets of MIC relations cover similar m_1 values but the visual–NIR colors – panels a), b), c) – show a stronger sensitivity in the faint magnitude limit and an almost linear change when moving from metal-poor to metal-rich stellar structures. The Strömgren colors – panels d), e), f) – show a minimal sensitivity for stellar structures more metal-rich than $[M/H] \gtrsim -0.25$. Moreover and even more importantly, the slopes of the MIC relations based on visual–NIR colors are on average shallower than the MIC relations based on Strömgren colors. This means that the former indices have, at fixed m_1 value, a stronger temperature sensitivity. We performed the same comparison with the α -enhanced models obtaining very similar results.

MIC relations for RG stars based on Strömgren colors are affected by the presence of molecular bands, such as CN , CH and NH . As a matter of fact, two strong cyanogen molecular absorption bands are located at $\lambda = 4142$ and $\lambda = 4215$ Å, i.e. very close to the effective wavelength of the v filter ($\lambda_{eff} = 4110$, $\Delta\lambda = 190$ Å). Moreover, the strong CH molecular band located in the Fraunhofer’s G -band ($\lambda = 4300$ Å) might affect both the v and the b magnitude. It is noteworthy that the molecular NH band at $\lambda = 3360$ Å, and the two CN bands at $\lambda = 3590$ and $\lambda = 3883$ Å might affect the u ($\lambda_{eff} = 3450$, $\Delta\lambda = 300$ Å) magnitude (see, e.g. Smith 1987). To decrease the contamination by molecular bands in the color index, we decided to adopt only colors based on the y -band and on the NIR bands in our new calibration of MIC relations. The main advantage of this approach is that the aforementioned molecular bands only affect the Strömgren m_1 index.

We derived theoretical MIC relations based on m_1 and the y -NIR colors based on 2MASS J, H, K filters. Together with the classical m_1 index, we also computed independent MIC relations for the reddening-free parameter $[m] = m_1 + 0.3 \times (b - y)$, to overcome deceptive uncertainties caused by differential reddening. To select the m_1 and the $[m]$ values along the individual isochrones we followed the same approach adopted in CA07. A multilinear regression fit was performed to estimate the coefficients of the MIC relations for the m_1 and the $[m]$ indices as a function of the three CIs , namely $y - J, y - H$ and $y - K$:

$$m_1 = \alpha + \beta [M/H] + \gamma CI + \delta CI^2 + \epsilon m_1^2 + \zeta (CI \times [M/H]) + \eta (m_1 \times [M/H]) + \theta (CI \times m_1) +$$

⁴ The complete set of BCs, CTRs and the Vega flux are available at <http://www.user.oat.ts.astro.it/castelli>

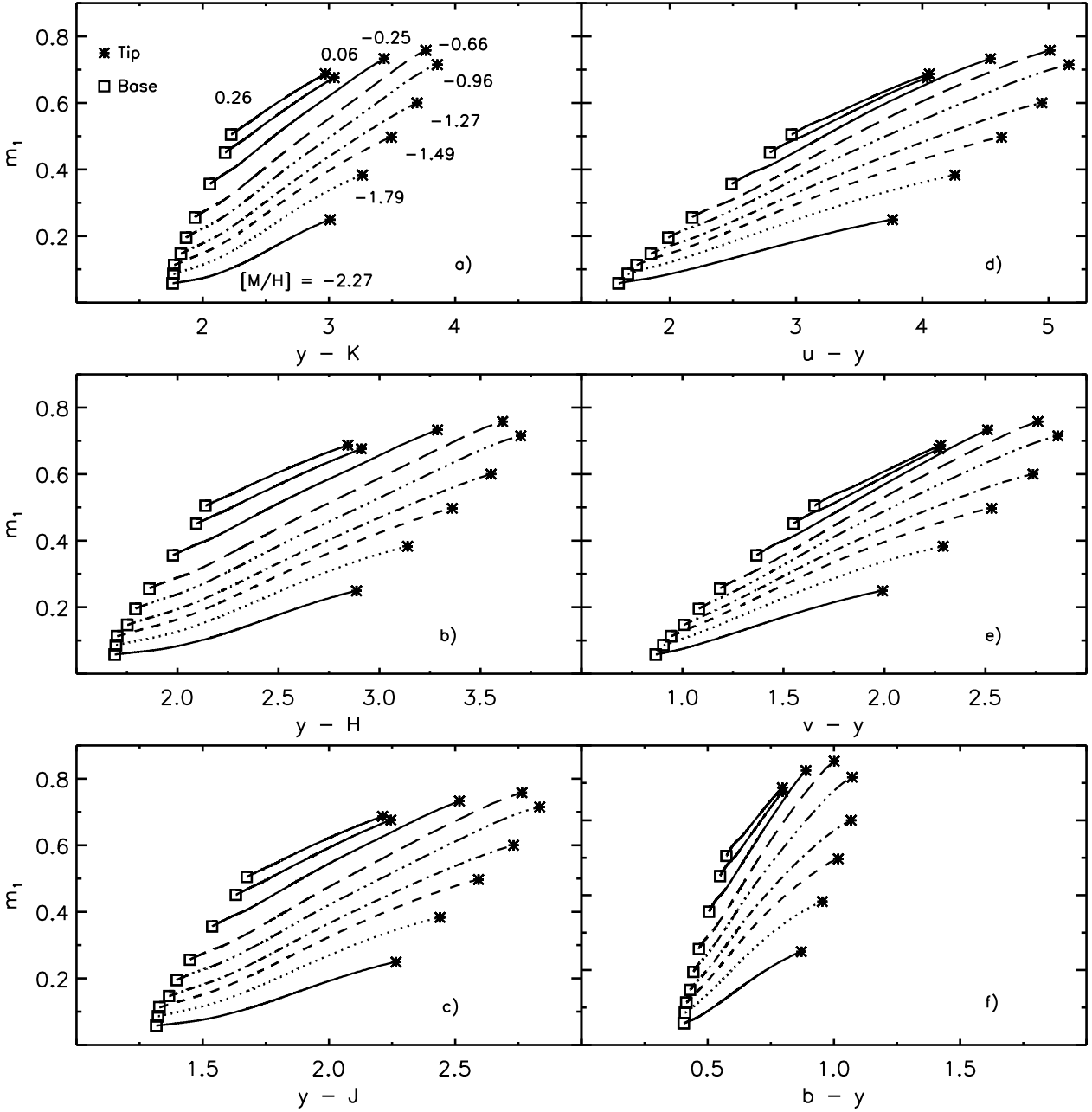


Fig. 8. Left panels – m_1 vs $y - K$ plane [panel a)] for isochrones at fixed cluster age ($t = 12$ Gyr) and different global metallicities ($[M/H]$, see labeled values). The evolutionary phases range from \approx the base (empty squares) to \approx the tip of the RGB (asterisks). Evolutionary tracks were computed by assuming a scaled-solar chemical mixture and transformed into the observational plane by adopting atmosphere models computed assuming the same mixture. The panels b) and c) show similar relations, but in the m_1 vs $y - H$ and in the m_1 vs $y - J$ plane. Right panels – Same as the left, but for the m_1 vs $u - y$ [panel d)], m_1 vs $v - y$ [panel e)], m_1 vs $b - y$ [panel f)] planes.

$$\iota (CI^2 \times m_1^2)$$

where the symbols have their usual meaning. To select the form of the analytical relation we followed the forms adopted for the m_1 and the hk metallicity index calibrations in CA07 and Calamida et al. (2011), respectively. We performed several tests finding the best solution of the multilinear regression fit when adopting the m_1 index as an independent variable. We then selected the solution with the lowest chi-square of the multilinear regression fit. As a further check, we estimated the Root Mean Square (RMS) deviations of the fitted points from the fit and the

values range between 0.0005 to 0.0009. Moreover, the multi-correlation parameters attain values close to 1. The coefficients of the fits, together with their uncertainties, for the twelve MIC relations, are listed in Table 2. The RMS values and the multi-correlation parameters of the different relations are listed in the last two columns of the table.

The above MIC relations are valid in the following color ranges, $0.05 < m_1 < 0.7$ mag, $0.2 < [m] < 1.1$ mag, $1.4 < y - J < 2.8$ mag, $1.8 < y - H < 3.5$ mag, and $1.9 < y - K < 3.7$ mag, for the scaled-solar models, while in the following color ranges, $0.05 < m_1 < 0.6$ mag, $0.2 < [m] < 0.9$ mag, $1.5 < y - J < 2.7$

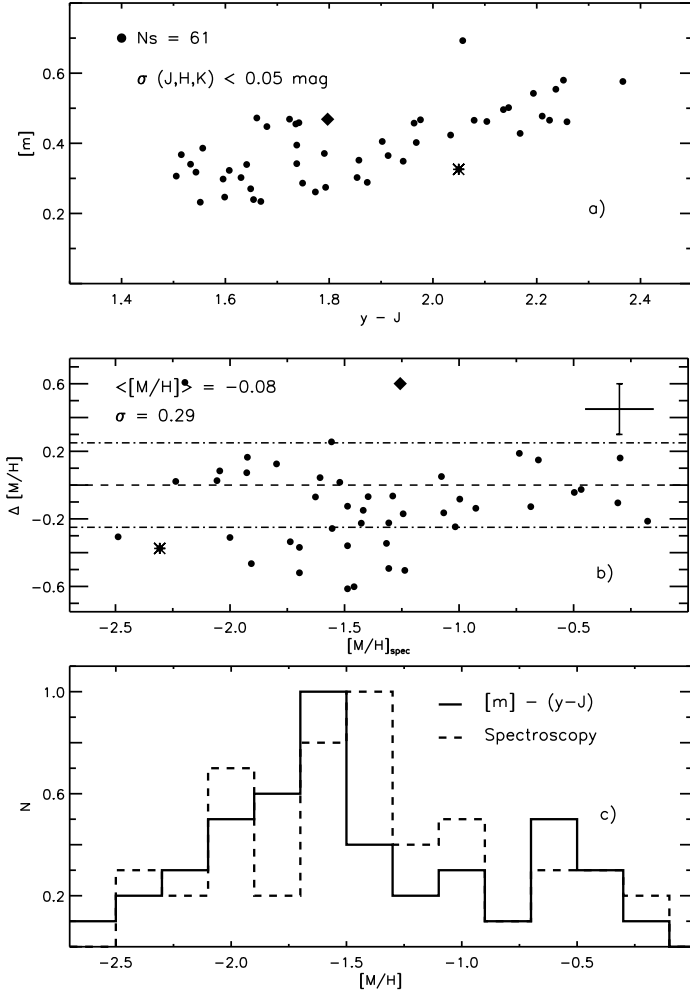


Fig. 9. Panel a) Selected field RGs from the sample of ATT94/ATT98 plotted in the $[m]$, $y - J$ plane ($N_s = 61$, filled dots). Panel b) Difference between photometric and spectroscopic metallicities, $\Delta[M/H] = [M/H]_{\text{phot}} - [M/H]_{\text{spec}}$, plotted versus $[M/H]_{\text{spec}}$ for the 61 field RGs (filled dots). Photometric metallicities are based on the α -enhanced $[m]$, $y - J$ MIC relation. Panel c) Normalized photometric metallicity distribution for the 61 RGs obtained with the $[m]$, $y - J$ MIC relation (black solid line), compared to the normalized spectroscopic distribution (black dashed).

mag, $2.0 < y - H < 3.5$ mag, and $2.0 < y - K < 3.7$ mag, for the α -enhanced models.

6. Validation of the new metallicity calibration

6.1. Field red-giant stars

In order to validate the new theoretical calibration of the m_1 index based on visual–NIR colors we estimate the metallicity of field RGs for which $uvby$ and NIR photometry and high-resolution spectroscopy are available. The Strömgren photometry and the spectroscopy is from Anthony-Twarog & Twarog (1994, 1998, hereafter ATT98), while NIR data were retrieved from the 2MASS archive (see CA07 for more details on the selection of this sample). The sample includes 81 field RGs with a measurement in the $uvby$ and the J, H, K bands, a reddening estimate (ATT98) and high-resolution spectroscopy in the Zinn & West (1984) metallicity scale. For 28 RGs we retrieved⁵ the *Calcium* abundance from Fulbright (2000), from which a proxy of the α -enhancement is

estimated, i.e. $[\alpha/Fe] \approx [Ca/Fe]$. We apply the α -enhanced calibration since we verified that it is the best suited to estimate the photometric metallicity of halo field RGs (Calamida et al. 2012, CA07). The metallicity range covered by current α -enhanced MIC relations is $-2.3 < [M/H] < 0.3$ but we select stars with $-2.5 < [M/H] < 0.5$ to account for current uncertainties in spectroscopic abundances and in the GC metallicity scale (Kraft & Ivans 2003). Furthermore, we select the RGs in photometric accuracy, i.e. $\sigma_{J,H,K} < 0.05$ mag, and according to the color range of validity of the six MIC relations, ending up with a sample of 61 stars, for 12 of which we have the $[\alpha/Fe]$ spectroscopic measurement.

To un-redden the m_1 index and the colors of the field RGs we adopt $E(m_1) = -0.30 \times E(b-y)$ (CA07), and $E(y - J) = 2.23 \times E(B - V)$, $E(y - H) = 2.56 \times E(B - V)$, $E(y - K) = 2.75 \times E(B - V)$, estimated assuming the Cardelli et al. (1989) reddening relation and $R_V = A_V/E(B - V) = 3.1$.

The selected stars are plotted in the $[m]$, $y - J$ plane in panel a) of Fig. 9 (filled dots). The star marked with an asterisk is HD 84903, which might be affected by weak chromospheric emission in the core of the *CaIIK* line (ATT98). For this star we adopt the spectroscopic measurement by

⁵ Data have been retrieved from the VO database using Topcat.

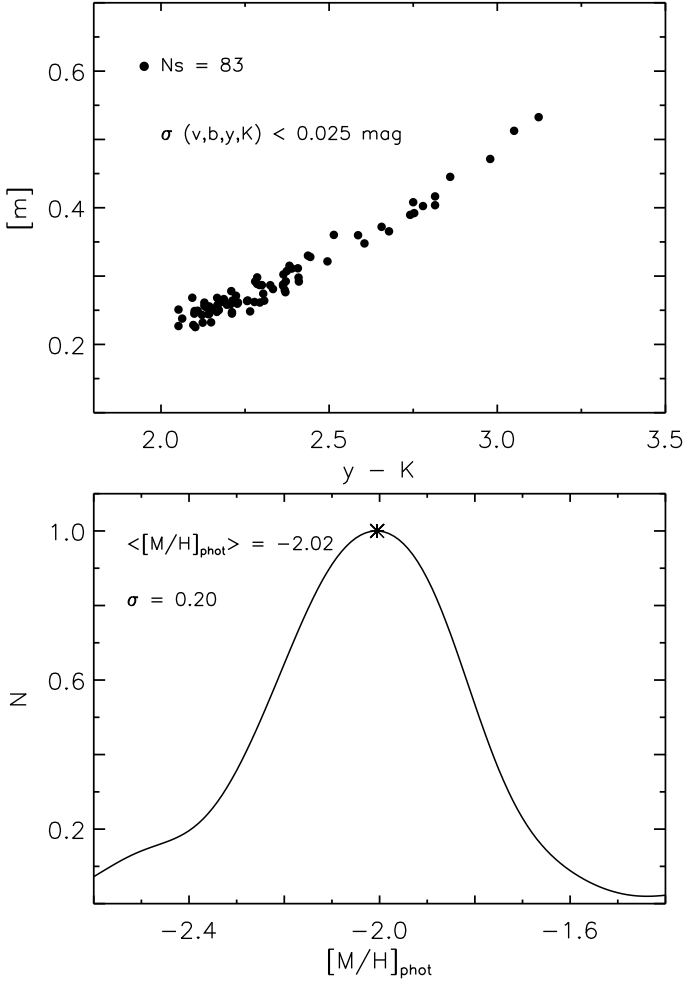


Fig. 10. Top: selected RG stars of the GGC M 92 plotted in the $[m]$, $y - K$ plane. Bottom: photometric metallicity distribution obtained by applying the $[m]$, $y - K$ MIC relation for the sample 83 RG stars.

Thèvenin & Idiart (1999), estimated by accounting for non-LTE effects (Calamida et al. 2011). The diamond marks a CH-strong star, HD 55496 (ATT98, CA07). Panel b) of the same figure shows the difference between the photometric and the spectroscopic metallicity ($\Delta[M/H] = ([M/H]_{\text{phot}} - [M/H]_{\text{spec}})$) for the 61 field RG stars as a function of their spectroscopic metal abundances ($[M/H]_{\text{spec}}$). We assumed an α -enhancement of $[\alpha/\text{Fe}] = 0.4$ and estimated $[M/H]_{\text{spec}} = [\text{Fe}/\text{H}]_{\text{spec}} + \log(0.638 \times f + 0.362)$, where $\log(f) = [\alpha/\text{Fe}]$, for stars with no α -element abundance measurement. The observed dispersion is mainly due to photometric, reddening, and spectroscopic errors. The error bars in panel b) display the mean error for the spectroscopic abundance measurements (see ATT98 and CA07 for more details on how the errors are estimated). Data plotted in panel b) show that on average there seems to be a shift of photometric metal abundances towards metal-poor values. Photometric metallicities are estimated by adopting the $[m]$, $y - J$ MIC relation and the mean difference between photometric and spectroscopic measurements is -0.08 ± 0.10 dex, with a mean intrinsic dispersion of $\sigma = 0.29$ dex. The CH-strong star (diamond) shows a much higher photometric metallicity ($\Delta[M/H] = [M/H]_{\text{phot}} - [M/H]_{\text{spec}} = 0.6$) as expected (CA07). The difference between photometric and spectroscopic measurements de-

rived averaging the MIC relations based on the reddening free metallicity indices ($[m]$, $y - J$, $[m]$, $y - H$, $[m]$, $y - K$) is -0.13 ± 0.06 dex. Similar results are obtained when applying the other MIC relations, and the mean difference derived averaging the m_1 , $y - J$, m_1 , $y - H$, m_1 , $y - K$ relations is -0.16 ± 0.05 dex. In spite of this systematic small shift towards metal-poor values, the average intrinsic dispersions are $\sigma = 0.25$ and $\sigma = 0.24$ dex, respectively. Moreover, the shape of the photometric metallicity distribution estimated by adopting the $[m]$, $y - J$ relation agrees quite well, within uncertainties, with the shape of the spectroscopic one (see solid and dashed lines in panel c). A similar agreement between photometric and spectroscopic metallicity distributions is obtained when applying the other MIC relations.

A culprit for the systematic shift between photometric and spectroscopic abundances might be an α -enhancement for field stars smaller than the assumed α value. The evolutionary models adopted to perform our theoretical metallicity calibration have been computed assuming $[\alpha/\text{Fe}] = 0.4$. This is the typical enhancement found in cluster stars using high-resolution spectra (Kraft 1994; Gratton et al. 2004). Unluckily, we do not have an α -enhancement abundance measurement for our field star sample but only an estimate of the α -enhancement proxy, i.e. $[\alpha/\text{Fe}] \approx [\text{Ca}/\text{Fe}]$, for 12 out of the 61 RGs, with a median value of $[\alpha/\text{Fe}] = 0.35$, and a dispersion of 0.08 dex. It is worth mentioning that we were finding a similar shift, ≈ -0.1 dex, when adopting the visual–NIR α -enhanced MIC relations to estimate photometric metallicities of field dwarfs in Calamida et al. (2012). When assuming an α -enhancement of 0.2 for the stars without the $[\alpha/\text{Fe}]$ spectroscopic estimate, we find a very good agreement between spectroscopic and photometric abundance estimates. We obtain a mean difference of 0.04 ± 0.05 dex, with a mean intrinsic dispersion of $\sigma = 0.30$ dex ($[m]$, $y - J$, $[m]$, $y - H$, $[m]$, $y - K$) and 0.00 ± 0.05 dex, with $\sigma = 0.30$ dex (m_1 , $y - J$, m_1 , $y - H$, m_1 , $y - K$). On the other hand, when adopting the scaled-solar calibration to estimate the abundance of the same sample we obtain photometric metallicities systematically more metal-poor than the spectroscopic abundances, with a mean difference of -0.19 ± 0.04 and a mean dispersion of $\sigma = 0.26$ dex for the $[m]$, CI relations, while a mean difference of -0.24 ± 0.02 and a mean dispersion of $\sigma = 0.21$ dex for the m_1 , CI relations.

6.2. Cluster red-giant stars

To further validate the new theoretical visual–NIR metallicity calibration, we also adopt the photometry of a metal-poor halo GGC, M 92 (NGC 6341, $[\text{Fe}/\text{H}] = -2.35 \pm 0.05$, Carretta et al. 2009) and of a metal-rich bulge cluster, NGC 6624 ($[\text{Fe}/\text{H}] = -0.69 \pm 0.02$, Valenti et al. 2011).

The use of cluster data brings forward three indisputable advantages:

- The evolutionary status (age, effective temperature, surface gravity, stellar mass) of cluster RGs is well established.
- The abundance of iron and α -elements is known with high-precision.
- The selected clusters cover a broad range in iron abundance.

Data for NGC 6624 were collected with EFOSC2 during July 12 and 13 2010. We have u -, $8v$ -, $6b$ - and $4y$ -band images, with exposure times ranging between 40 to 380s and seeing between $1''.0$ to $1''.5$. The total FoV is $4.6' \times 4.6'$ and includes the cluster center. We followed the same approach adopted for NGC 6528 in reducing and calibrating the data, ending up with a catalog of 6,217 stars. These data were matched with

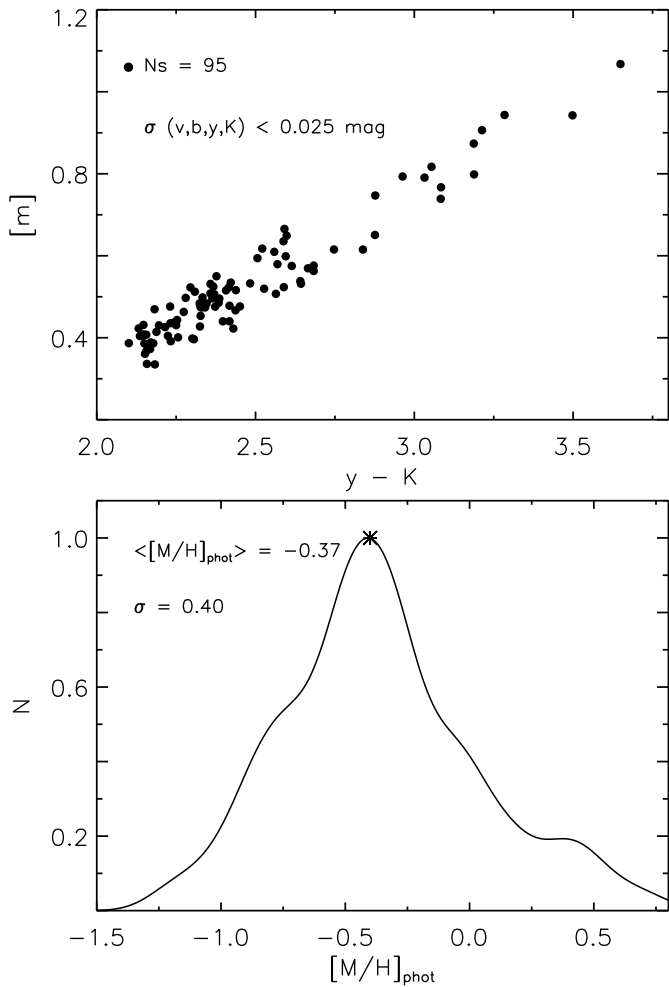


Fig. 11. Top: selected RGs of the bulge cluster NGC 6624 plotted in the $[m]$, $y - K$ plane. Bottom: photometric metallicity distribution obtained by applying the $[m]$, $y - K$ MIC relation for the sample of 95 RGs.

NIR VIRCAM photometry, obtaining an optical–NIR catalog of 4,252 stars.

The Strömgren catalog of M 92 was obtained with images collected with the 2.56m Nordic Optical Telescope (NOT) on La Palma (for more details see Grundahl et al. 2000, CA07). We cross-correlated the Strömgren photometry of M 92 with the NIR photometry of Valenti et al. (2004a) for the RGs in this cluster, ending up with a sample of 340 stars with a measurement in the u , v , b , y and J , K bands. We then adopted the $b - J$, $y - K$ color–color plane to disentangle the M 92 RGs from field stars as described in CA07, obtaining a clean cluster sample of 223 stars. We applied the same procedure to disentangle NGC 6624 RGs from field stars, ending up with a sample of 147 RGs for this cluster.

The top panel of Fig. 10 shows M 92 candidate member RGs selected in photometric accuracy, i.e. $\sigma_{v,b,y,K} < 0.025$ mag, and plotted in the $[m]$, $y - K$ plane; We adopted $E(B - V) = 0.02$ mag for M 92 (Di Cecco et al. 2010) and the relations derived in §5 to un-redden the cluster photometry. The bottom panel shows the metallicity distribution obtained for the 86 RGs by adopting the $[m]$, $y - K$ α -enhanced MIC relation. The distribution was smoothed by applying a Gaussian kernel having a standard deviation equal to the photometric error

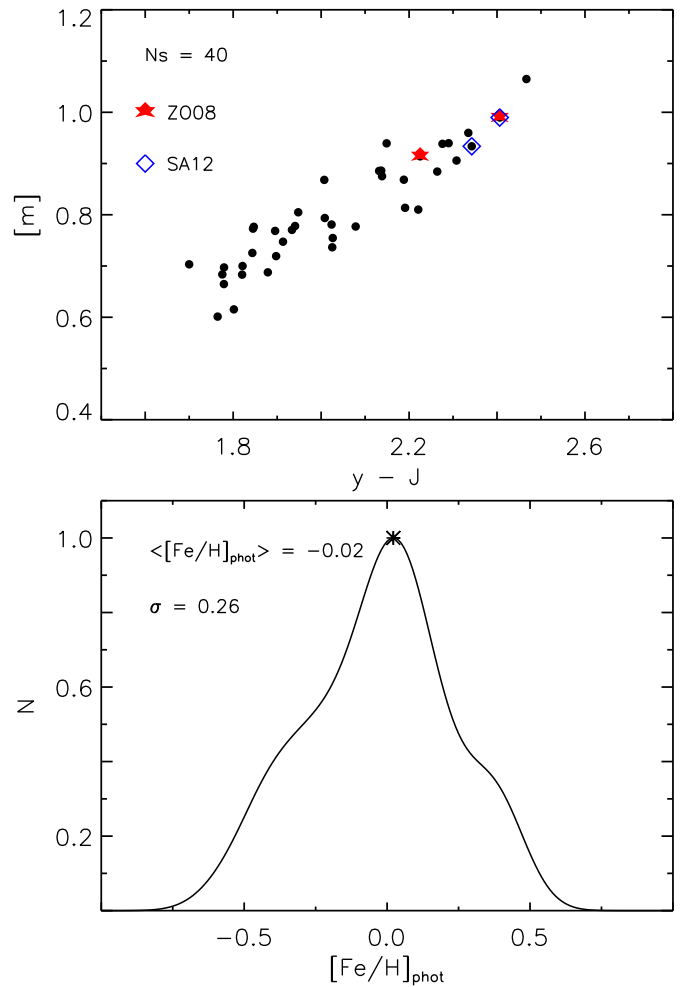


Fig. 12. Top: selected RGs of the bulge cluster NGC 6528 plotted in the $[m]$, $y - J$ plane. Bottom: photometric metallicity distribution obtained by applying the $[m]$, $y - J$ MIC relation for the sample of 40 RGs. Stars with spectroscopic measurements by Z08 and SA12 are marked with filled red stars and open blue diamonds, respectively.

in the m_1 index, following the prescriptions of Calamida et al. (2009, 2012). The distribution has a quite symmetric shape, and most of the spread is due to photometric errors. The residual spread is due to the effect of $CN/CH/NH$ molecular bands on the m_1 index; M 92 shows the typical variations in $[C/Fe]$ and $[N/Fe]$ (Carbon et al. 1982; Langer et al. 1986; Bellman et al. 2001), together with the usual anti-correlations of most GGCs (Pilachowski et al. 1983; Sneden et al. 1991; Kraft 1994). We also found a similar effect when applying the visual–NIR metallicity calibration to M 92 MS stars (Calamida et al. 2012).

By fitting it with a Gaussian we obtain a main peak at $[M/H] = -2.02$ ($[Fe/H] = -2.37$), with a dispersion of $\sigma = 0.20$ dex. The metallicity distributions obtained by applying the other MIC relations agree with each other, with averaged mean peaks of -2.05 ± 0.04 ($[Fe/H] = -2.40$) and a mean intrinsic dispersion of $\sigma = 0.31$ dex ($[m]$, $y - J$, $[m]$, $y - K$ relations), and of -2.07 ± 0.01 ($[Fe/H] = -2.42$), with $\sigma = 0.25$ dex (m_1 , $y - J$, m_1 , $y - K$ relations). These estimates are in good agreement, within uncertainties, with spectroscopic estimates from the literature ($[Fe/H] = -2.24 \pm 0.10$, Zinn & West 1984, and $[Fe/H] = -2.35 \pm 0.05$, Carretta et al. 2009). On the other hand, when ap-

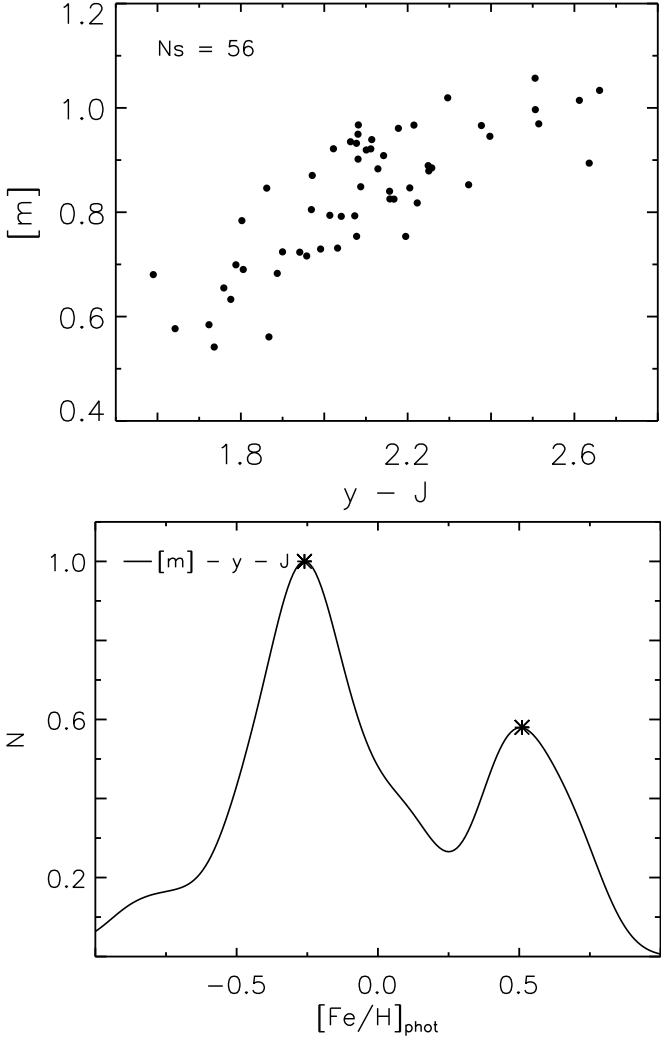


Fig. 13. Top: selected RGs of the field surrounding NGC 6528 in the Baade’s window plotted in the $[m]$, $y - J$ plane. Bottom: photometric metallicity distribution obtained by applying the $[m]$, $y - J$ MIC relation to the sample of 56 Baade’s window RGs. Stars with spectroscopic measurements by GO11 are marked with filled red stars.

plying the scaled-solar MIC relations to estimate the iron abundance of M 92, we obtain a mean peak of ($[Fe/H] = -2.17 \pm 0.01$, and a mean intrinsic dispersion of $\sigma = 0.24$ dex ($[m]$, $y - J$, $[m]$, $y - K$ relations), and of -2.15 ± 0.02 , with $\sigma = 0.40$ dex (m_1 , $y - J$, m_1 , $y - K$ relations). These values are on average slightly (~ 0.1 dex) more metal-rich than the spectroscopic values.

Fig. 11 shows the same test performed for NGC 6624. We adopted a reddening of $E(B - V) = 0.28$ mag for this cluster (Valenti et al. 2004a). The candidate RGs clearly split in two sequences in the $[m]$, $y - K$ plane (see top panel). The split is due to the effect of the molecular bands, such as CN , CH and NH , on the m_1 index, that is more pronounced in metal-rich clusters, as shown in CA07, and constrained by ACS-HST photometry in the case of NGC 1851 and 47 Tuc (Milone et al. 2008, 2012). The presence of this dichotomy in NGC 6624 has not yet been confirmed by spectroscopic studies.

The smoothed metallicity distribution obtained by applying the $[m]$, $y - K$ α -enhanced MIC relation is shown in the bot-

tom panel of Fig. 11. The shape of the distribution is asymmetric, with a tail towards the metal-rich regime up to $[M/H] \approx 0.7$, and a secondary peak at $[M/H] \approx 0.4$. The metal-rich tail could be due to the residual contamination by field disk stars. Fitting the distribution with a single Gaussian we obtain a main peak at $[M/H] = -0.37$ ($[Fe/H] = -0.72$), with a dispersion of $\sigma = 0.40$ dex. Most of the dispersion is due to photometric errors, but part of it is due to the presence of uncorrected differential reddening and the rest is intrinsic, i.e. given to the presence of CN -, CH -strong stars. The metallicity distributions obtained by applying the other MIC relations agree with each other, with averaged mean peaks of -0.39 ± 0.09 ($[Fe/H] = -0.74$) and a mean intrinsic dispersion of $\sigma = 0.42$ dex ($[m]$, $y - J$, $[m]$, $y - H$, and $[m]$, $y - K$ relations), and of -0.40 ± 0.04 ($[Fe/H] = -0.75$), with $\sigma = 0.42$ dex (m_1 , $y - J$, m_1 , $y - H$, and m_1 , $y - K$ relations). These estimates are in good agreement, within uncertainties, with high-resolution spectroscopic estimates from Valenti et al. (2011), $[Fe/H] = -0.69 \pm 0.02$, and with the CaT measurements of Heasley et al. (2000), $[Fe/H] = -0.63 \pm 0.09$, and of Mauro et al. (2014), $[Fe/H] = -0.67 \pm 0.10$. On the other hand, by applying the scaled-solar metallicity relations to estimate the cluster iron abundance we obtain an average mean peak of $[Fe/H] = -0.97 \pm 0.03$ and a mean intrinsic dispersion of $\sigma = 0.28$ dex ($[m]$, $y - J$, $[m]$, $y - H$, and $[m]$, $y - K$ relations), and of -0.99 ± 0.06 , with $\sigma = 0.34$ dex (m_1 , $y - J$, m_1 , $y - H$, and m_1 , $y - K$ relations). These iron abundances are almost 0.3 dex more metal-poor than the spectroscopic values.

7. The metallicity of the bulge cluster NGC 6528 and its surrounding field.

We adopt the new visual–NIR calibration to estimate the metal abundance of the bulge cluster NGC 6528 and to study the metallicity distribution of RGs in the surrounding field in the Baade’s window.

We select 97 RG stars from the clean cluster sample shown in Fig. 2. Stars are further selected in photometric accuracy, i.e. $\sigma_{v,b,y,J,H,K} \leq 0.025$ mag, separation index, $sep_{v,b,y} \geq 5$, and for the color ranges of validity of the calibration, obtaining a final sample of 40 NGC 6528 RGs. We adopted $E(B - V) = 0.54$ mag to un-redden the data (see §4). The top panel of Fig. 12 shows the selected stars plotted in the $[m]$, $y - J$ plane. The two filled red stars mark RGs with high-resolution spectroscopic measurement from ZO08 and the empty blue diamonds mark two RGs with CaT spectroscopic abundances from SA12. One star, I 42, belongs to both samples. Four stars from the sample of SA12 were rejected since they did not pass the selection in photometric accuracy or they were outside the color range of validity of the calibration. The dispersion of the sequence in the $[m]$, $y - J$ plane is mostly due to photometric errors, and possibly to some residual uncorrected differential reddening. It is noteworthy that RGs do not split in two parallel sequences in this color–color plane, as in the case of NGC 6624. Unfortunately, we do not have enough statistics to ascertain if the absence of the split is intrinsic or given to the effect of the paucity of the sample. We also do not have enough spectroscopic data to constrain the effect of $CN/CN/NH$ molecular bands on the broadening of the RG sequence in the $[m]$, $y - J$ plane.

The smoothed metallicity distribution obtained by applying the scaled-solar $[m]$, $y - J$ MIC relation is shown in the bottom panel of Fig. 12. The shape of the distribution is quite similar to the shape of the metallicity distribution of NGC 6624, while the dispersion is much lower, $\sigma = 0.19$ dex compared to $\sigma = 0.40$ dex. Part of the difference could be due to the fact that NGC 6528

Strömgren–NIR catalog was corrected for differential reddening and cleaned from the contamination of field disk stars by using proper-motion measurements estimated with HST photometry, while NGC 6624 catalog was cleaned by field contamination only by adopting the Strömgren–NIR color–color planes, and it was not corrected for differential reddening. The metal-rich tail present in the NGC 6624 metallicity distribution is indeed absent in the NGC 6528 distribution, but the distribution does not look to be mono-parametric. Fitting NGC 6528 MDF with a single Gaussian we obtain a main peak at $[\text{Fe}/\text{H}] = -0.02$, with a dispersion of $\sigma = 0.19$ dex, by adopting the scaled-solar $[m]$, $y - J$ MIC relation. The metallicity distributions obtained by applying the other scaled-solar MIC relations agree with each other, with average mean peaks of -0.04 ± 0.02 and a mean intrinsic dispersion of $\sigma = 0.27$ dex ($[m]$, $y - J$ and $[m]$, $y - K$ relations), and of -0.11 ± 0.01 , with $\sigma = 0.27$ dex (m_1 , $y - J$ and m_1 , $y - K$ relations). The photometric metallicity estimates for the four RGs with the corresponding spectroscopic measurements from ZO08 and SA12 are listed in Table 3, together with the spectroscopic measurement errors. For star I 42 we estimated α -enhancement as $[\alpha/\text{Fe}] = [\text{Ca} + \text{Mg} + \text{Si}/\text{Fe}]$. The reduced equivalent widths $-W'$ from SA12 were converted to $[\text{Fe}/\text{H}]$ measurements by adopting the relation presented in the paper (the interested reader is referred to SA12 for more details), and then converted to the Zinn & West (1984) metallicity scale by adopting the relation provided by Carretta et al. (2009). The agreement between photometric and spectroscopic estimates for the four RGs is very good within the uncertainties (see Table 3).

We adopted also the α -enhanced MIC relations to estimate the metallicities of NGC 6528 RGs but we obtained metal abundances of more than 0.5 dex too metal-rich, i.e. $\Delta[\text{M}/\text{H}] = [\text{M}/\text{H}]_{\text{phot}} - [\text{M}/\text{H}]_{\text{spec}} \approx 0.5$ dex.

We then adopted our clean sample of bulge stars to study the metallicity distribution of the Baade’s window. We selected RG stars from the sample shown in Fig. 4, ending up with 62 candidate bulge RGs. The stars are then further selected in photometric accuracy, i.e. $\sigma_{v,b,y,J,H,K} \leq 0.03$ mag and separation index, $sep_{v,b,y} \geq 0$, and for the color ranges of validity of the calibration, obtaining a final sample of 56 RGs. The sample photometry has been un-reddened by using the same reddening adopted for NGC 6528. The top panel of Fig. 12 shows the selected stars plotted in the $[m]$, $y - J$ plane. The bottom panel of Fig. 12 displays the smoothed photometric metallicity distribution obtained by applying the scaled-solar $[m]$, $y - J$ MIC relation. The distribution is clearly bimodal, with a main peak at $[\text{Fe}/\text{H}] \approx -0.25$ and a secondary one at $[\text{Fe}/\text{H}] \approx 0.5$. Similar distributions are obtained when adopting the other visual–NIR MIC relations, with average peaks at $[\text{Fe}/\text{H}] \approx -0.2$ and $[\text{Fe}/\text{H}] \approx 0.55$ ($[m]$, $y - J$, $[m]$, $y - H$ and m_1 , $y - K$ relations), and $[\text{Fe}/\text{H}] \approx -0.25$ and $[\text{Fe}/\text{H}] \approx 0.4$ (m_1 , $y - J$, m_1 , $y - H$, and m_1 , $y - K$ relations). By applying the α -enhanced MIC relations we obtain a metallicity distribution shifted by almost 1 dex towards the metal-rich regime.

8. Summary and conclusions

We presented Strömgren–NIR photometry of the the bulge globular cluster NGC 6528 and its surrounding field in the Baade’s window. The main findings concerning Strömgren–NIR photometry of cluster and field stars are the following:

a) The isochrone fit of the proper-motion-cleaned and differential reddening corrected Strömgren–NIR CMDs for NGC 6528 suggests an age of 11 ± 1 Gyr, by adopting a scaled-solar isochrone with solar abundance, i.e. $Z = 0.0198$, $Y =$

0.273, or a α -enhanced isochrone with the same iron content, i.e. $Z = 0.04$, $Y = 0.303$. The same scaled-solar and α -enhanced isochrones agree quite well, within the uncertainties, with the NIR CMD of NGC 6528. This result is in good agreement with literature age estimates, i.e. $t = 11 \pm 2$ Gyr (Feltzing & Johnson 2002), 12.6 Gyr (Momany et al. 2003), and 11 ± 1 Gyr (LA14).

b) We adopted the same theoretical framework used for NGC 6528 to fit Strömgren–NIR CMDs of proper-motion selected and differential reddening corrected bulge stars. We find that a fraction of observed stars along the MS and the RGB are systematically redder and/or fainter than predicted by adopted cluster isochrones. This result would suggest the possible occurrence of large samples of super metal-rich stars, $[\text{Fe}/\text{H}] > 0.1$, in the Baade’s window. However, these objects could also be explained with an increase either in differential reddening or in depth or both.

c) We find that central helium burning stars display a well defined double peak distribution. The fainter peak is located at $K \sim 13.25 \pm 0.02$ and appears to be associated with the RHB stars, since the peak in the K -band luminosity function of cluster RGs is located at $K \sim 13.16 \pm 0.02$ mag. The brighter ($K \sim 12.86 \pm 0.02$) peak seems to be associated with intermediate-age RC stars. The two peaks also show a clear separation in color (RHB, J-K ~ 1.0 ; RC, J-K ~ 0.9). More quantitative constraints concerning the age and the metallicity distribution of the above evolutionary features do require detailed synthetic CMDs and luminosity functions (Calamida et al., in preparation).

Furthermore, we also provided a new theoretical metallicity calibration based on the m_1 index and on visual–NIR colors to estimate the global metal abundance of cluster and field RG stars. We adopted scaled-solar and α -enhanced evolutionary models. This is the first time that visual–NIR colors are adopted to estimate photometric metallicities of RG stars.

We validated the new theoretical metallicity calibration by adopting a sample of field RGs with Strömgren and NIR photometry and high-resolution spectroscopy available. The sample includes 61 RGs selected from the study by ATT94 and ATT98. The mean difference between photometric and spectroscopic abundance is -0.16 ± 0.05 dex, with a mean intrinsic dispersion of $\sigma = 0.24$ dex (m_1 , $y - J$, and m_1 , $y - K$ relations), and 0.13 ± 0.06 dex, with $\sigma = 0.25$ dex ($[m]$, $y - J$ and $[m]$, $y - K$ relations).

The quoted independent comparisons indicate that the new theoretical MIC relations provide accurate metal abundances for field RG stars with a dispersion smaller than 0.3 dex.

We also tested the calibration by adopting RG stars of two GGCs covering a broad range in metal abundance, i.e. M 92 ($[\text{Fe}/\text{H}] = -2.31$) and NGC 6624 ($[\text{Fe}/\text{H}] = -0.69$), for which both Strömgren and NIR photometry were available.

We find that the metallicity distributions of M 92 based on the α -enhanced visual–NIR MIC relations are in very good agreement with the spectroscopic estimates available in literature, i.e. $[\text{Fe}/\text{H}] = -2.24 \pm 0.10$ (Zinn & West 1984), and $[\text{Fe}/\text{H}] = -2.35 \pm 0.05$ (Carretta et al. 2009). We find, indeed, a global metallicity of $[\text{M}/\text{H}] = -2.05 \pm 0.04$ ($[\text{Fe}/\text{H}] = -2.40$), with a mean intrinsic dispersion of $\sigma = 0.31$ dex, by averaging the values obtained by adopting the $[m]$, $y - J$ and the $[m]$, $y - K$ relations, and of -2.07 ± 0.01 ($[\text{Fe}/\text{H}] = -2.42$), with $\sigma = 0.25$ dex, by using the m_1 , $y - J$ and m_1 , $y - K$ relations.

By applying the α -enhanced visual–NIR MIC relations to the bulge cluster NGC 6624 we find averaged mean peaks of -0.39 ± 0.09 ($[\text{Fe}/\text{H}] = -0.74$) and a mean intrinsic dispersion of $\sigma = 0.42$ dex ($[m]$, $y - J$, $[m]$, $y - H$, and $[m]$, $y - K$ relations), and of -0.40 ± 0.04 ($[\text{Fe}/\text{H}] = -0.75$), with $\sigma = 0.42$ dex

Table 1. Log of the Strömgren images collected with EFOSC2 on the NTT for the bulge cluster NGC 6528 and the halo cluster NGC 6752 adopted in this investigation (program ID: 085.D-0374, PI: A. Calamida).

Name	Exposure time (s)	Filter	RA (hh:mm:ss.s)	DEC (dd:mm:ss.s)	Seeing (arcsec)
NGC 6528					
July 11, 2010					
EFOSC.2010-07-12T03:49:59.514.fits	60	y	18:04:42.6	-30:04:56.9	0.8
EFOSC.2010-07-12T03:51:42.194.fits	200	b	18:04:42.6	-30:04:56.9	0.8
EFOSC.2010-07-12T03:55:45.076.fits	1000	v	18:04:42.6	-30:04:56.9	0.8
EFOSC.2010-07-12T04:13:08.053.fits	2000	u	18:04:42.6	-30:04:56.9	1.1
July 13, 2010					
EFOSC.2010-07-14T04:03:08.983.fits	60	y	18:04:38.5	-30:05:57.0	1.1
EFOSC.2010-07-14T04:04:47.581.fits	60	y	18:04:37.4	-30:06:11.9	1.1
EFOSC.2010-07-14T04:06:44.945.fits	300	b	18:04:38.5	-30:05:57.0	1.1
EFOSC.2010-07-14T04:12:27.376.fits	300	b	18:04:37.4	-30:06:11.9	1.2
EFOSC.2010-07-14T04:18:18.498.fits	2500	v	18:04:38.5	-30:05:57.0	1.5
EFOSC.2010-07-14T05:01:01.323.fits	2100	u	18:04:38.5	-30:05:57.0	1.7
NGC 6752					
July 11, 2010					
EFOSC.2010-07-12T03:14:57.815.fits	3	y	19:10:53.6	-59:59:21.4	1.2
EFOSC.2010-07-12T03:15:41.972.fits	3	y	19:10:51.7	-59:58:55.4	1.2
EFOSC.2010-07-12T03:16:27.729.fits	3	y	19:10:49.6	-59:59:21.3	1.2
EFOSC.2010-07-12T03:17:35.375.fits	6	b	19:10:53.6	-59:59:21.4	1.2
EFOSC.2010-07-12T03:18:23.873.fits	6	b	19:10:51.7	-59:58:55.4	1.2
EFOSC.2010-07-12T03:19:11.922.fits	6	b	19:10:49.6	-59:59:21.3	1.2
EFOSC.2010-07-12T03:20:21.398.fits	30	v	19:10:53.6	-59:59:21.4	1.2
EFOSC.2010-07-12T03:21:34.085.fits	30	v	19:10:51.7	-59:58:55.4	1.2
EFOSC.2010-07-12T03:22:44.113.fits	30	v	19:10:49.6	-59:59:21.3	1.2
EFOSC.2010-07-12T03:24:17.518.fits	60	u	19:10:53.6	-59:59:21.4	1.2
EFOSC.2010-07-12T03:26:00.197.fits	60	u	19:10:51.7	-59:58:55.4	1.2
EFOSC.2010-07-12T03:27:42.216.fits	60	u	19:10:49.6	-59:59:21.3	1.2
July 13, 2010					
EFOSC.2010-07-14T03:31:07.342.fits	10	y	19:10:53.6	-59:59:21.4	1.2
EFOSC.2010-07-14T03:31:59.032.fits	10	y	19:10:51.7	-59:58:55.4	1.2
EFOSC.2010-07-14T03:32:49.501.fits	10	y	19:10:49.6	-59:59:21.3	1.2
EFOSC.2010-07-14T03:34:01.889.fits	25	b	19:10:53.6	-59:59:21.4	1.2
EFOSC.2010-07-14T03:35:06.773.fits	25	b	19:10:51.7	-59:58:55.4	1.2
EFOSC.2010-07-14T03:36:11.228.fits	25	b	19:10:49.6	-59:59:21.3	1.2
EFOSC.2010-07-14T03:37:37.140.fits	60	v	19:10:53.6	-59:59:21.4	1.2
EFOSC.2010-07-14T03:39:18.139.fits	60	v	19:10:51.7	-59:58:55.4	1.2
EFOSC.2010-07-14T03:40:58.507.fits	60	v	19:10:49.6	-59:59:21.3	1.2
EFOSC.2010-07-14T03:42:58.503.fits	80	u	19:10:53.6	-59:59:21.4	1.2
EFOSC.2010-07-14T03:45:01.599.fits	80	u	19:10:51.7	-59:58:55.4	1.2
EFOSC.2010-07-14T03:47:01.975.fits	80	u	19:10:49.6	-59:59:21.3	1.2

Notes. This table is available in its entirety in a machine-readable form in the online journal.

($m_1, y-J, m_1, y-H$, and $m_1, y-K$ relations). These estimates are in good agreement, within uncertainties, with spectroscopic estimates from the literature ([Fe/H] = -0.63 ± 0.09 , Heasley et al. 2000, and [Fe/H] = -0.69 ± 0.02 , Valenti et al. 2011).

We also apply the new calibration to study the metallicity distribution of the bulge cluster NGC 6528 and its surrounding field. The smoothed metallicity distribution obtained by applying the scaled-solar $[m], y - J$ MIC relation to the proper-motion selected and differential reddening corrected cluster RGs shows a main peak at [Fe/H] = -0.02 , with a dispersion of $\sigma = 0.19$ dex. The metallicity distributions obtained by applying the other scaled-solar MIC relations agree with each other, with average mean peaks of -0.04 ± 0.02 and a mean intrinsic dispersion of $\sigma = 0.27$ dex ($[m], y - J$ and $[m], y - K$ relations), and of -0.11 ± 0.01 , with $\sigma = 0.27$ dex ($m_1, y - J$ and $m_1, y - K$ relations). The agreement between photometric and spectroscopic estimates for the four RGs in common with the spectroscopic samples of ZO04 and SA12 is, within the uncer-

ainties, very good. By adopting the α -enhanced MIC relations to estimate the metallicities of NGC 6528 RGs we obtain metal abundances of more than 0.5 dex too metal-rich, i.e. $\Delta[M/H] = [M/H]_{\text{phot}} - [M/H]_{\text{spec}} \approx 0.5$ dex. This result would support the spectroscopic measurements of ZO04 for NGC 6528, which give [Fe/H] = -0.10 ± 0.2 and a low α -enhancement, i. e. $[\alpha/\text{Fe}] \approx 0.1$, and the findings of Carretta et al. (2001), based on high-resolution spectroscopy of RHB stars, which give [Fe/H] = 0.07 ± 0.01 , with a modest α -enhancement, $[\alpha/\text{Fe}] \approx 0.2$.

The smoothed photometric metallicity distribution of proper-motion selected and differential reddening corrected RGs in the Baade’s window surrounding NGC 6528, based on scaled-solar $[m], y - J$ MIC relation, is clearly bimodal, with a main peak at [Fe/H] ≈ -0.25 and a secondary one at [Fe/H] ≈ 0.5 . Similar distributions are obtained when adopting the other visual–NIR MIC relations, with average peaks at [Fe/H] ≈ -0.2 and [Fe/H] ≈ 0.55 ($[m], y - J$, $[m], y - H$ and $m_1, y - K$ relations), and [Fe/H] ≈ -0.25 and [Fe/H] ≈ 0.4 ($m_1, y - J$, $m_1, y - H$, and

Table 2. Multilinear regression coefficients for the Strömgren metallicity index: $m_1 = \alpha + \beta [\text{Fe}/\text{H}] + \gamma CI + \delta CI^2 + \epsilon m_1^2 + \zeta (CI \times [\text{Fe}/\text{H}]) + \eta (m_1 \times [\text{Fe}/\text{H}]) + \theta (CI \times m_1) + \iota (CI^2 \times m_1^2)$

Relation	α	β	γ	δ	ϵ	ζ	η	θ	ι	Multicorr	RMS
Scaled-solar											
$m_1, y - J$	-0.107	0.133	0.365	-0.196	-0.715	-0.090	0.130	0.860	-0.012	1.000	0.0007
Error	0.002	0.007	0.004	0.043	0.002	0.006	0.018	0.001	0.006	(...)	(...)
$[m], y - J$	-0.138	0.132	0.500	-0.319	-0.918	-0.111	0.161	1.132	-0.004	1.000	0.0008
Error	0.002	0.007	0.005	0.041	0.002	0.006	0.026	0.001	0.005	(...)	(...)
$m_1, y - H$	-0.060	0.132	0.237	-0.104	-0.662	-0.068	0.133	0.649	-0.012	1.000	0.0007
Error	0.0014	0.004	0.002	0.042	0.001	0.006	0.013	0.001	0.004	(...)	(...)
$[m], y - H$	-0.103	0.137	0.361	-0.174	-0.528	-0.080	0.093	0.721	-0.006	1.000	0.0009
Error	0.0014	0.007	0.003	0.040	0.001	0.008	0.018	0.001	0.006	(...)	(...)
$m_1, y - K$	-0.068	0.137	0.239	-0.103	-0.719	-0.070	0.137	0.650	-0.009	1.000	0.0008
Error	0.0015	0.004	0.002	0.043	0.001	0.007	0.013	0.001	0.004	(...)	(...)
$[m], y - K$	-0.116	0.149	0.363	-0.155	-0.454	-0.077	0.084	0.637	-0.003	1.000	0.0008
Error	0.0015	0.007	0.003	0.045	0.001	0.008	0.021	0.001	0.007	(...)	(...)
α -enhanced											
$m_1, y - J$	-0.123	0.091	0.310	-0.137	-0.516	-0.053	0.075	0.687	-0.019	1.000	0.0005
Error	0.001	0.005	0.003	0.050	0.001	0.005	0.016	0.002	0.004	(...)	(...)
$[m], y - J$	-0.148	0.091	0.438	-0.232	-0.628	-0.065	0.084	0.869	-0.009	0.998	0.0006
Error	0.001	0.009	0.008	0.077	0.002	0.008	0.041	0.002	0.008	(...)	(...)
$m_1, y - H$	-0.094	0.099	0.220	-0.079	-0.467	-0.045	0.077	0.532	-0.014	1.000	0.0005
Error	0.008	0.003	0.002	0.054	0.001	0.006	0.014	0.001	0.004	(...)	(...)
$[m], y - H$	-0.131	0.093	0.331	-0.145	-0.550	-0.054	0.071	0.684	-0.008	1.000	0.0005
Error	0.001	0.004	0.003	0.039	0.001	0.005	0.016	0.005	0.004	(...)	(...)
$m_1, y - K$	-0.101	0.096	0.217	-0.076	-0.595	-0.044	0.090	0.543	-0.011	0.999	0.0005
Error	0.001	0.003	0.001	0.050	0.001	0.005	0.012	0.001	0.003	(...)	(...)
$[m], y - K$	-0.138	0.095	0.322	-0.127	-0.421	-0.048	0.058	0.596	-0.008	0.999	0.0005
Error	0.001	0.004	0.002	0.042	0.001	0.005	0.017	0.001	0.004	(...)	(...)

Table 3. Photometric and spectroscopic metallicities for four RG stars in the bulge cluster NGC 6528.

Name	$[\text{Fe}/\text{H}]_{m_1, yJ}$	$[\text{Fe}/\text{H}]_{[m], yJ}$	$[\text{Fe}/\text{H}]_{m_1, yK}$	$[\text{Fe}/\text{H}]_{[m], yK}$	$[\text{Fe}/\text{H}]_s$	$err([\text{Fe}/\text{H}]_s)$	$[\alpha/\text{Fe}]$
357459	-0.09	0.04	-0.24	-0.09	-0.01 ^a	0.29	(...)
142	-0.03	-0.04	0.26	-0.10	-0.14 ^a	0.075	0.09 ^a
R1-42	-0.03	-0.04	0.26	-0.10	-0.05 ^b	0.15	0.09 ^a
R2-41	0.05	-0.19	0.18	0.10	-0.15 ^b	0.15	(...)

Notes. ^a High-resolution spectroscopic measurement from Z008. ^b *CaT* spectroscopic measurement from SA12.

$m_1, y - K$ relations). By applying the α -enhanced MIC relations we obtain a metallicity distribution shifted by almost 1 dex towards the metal-rich regime.

The shape of our photometric metallicity distribution is quite similar to the shape of the spectroscopic distribution derived by Z008 and Hill et al. (2011) based on a sample of ≈ 200 RGs in the Baade’s window. The metal-rich peak of the photometric distribution is slightly shifted ($\approx 0.15 - 0.2$ dex) towards the metal-rich regime. The shift could be due to the effect of the molecular *CN/CH/NH*-bands on the m_1 index, so the RGs mimic to be more metal-rich than what they really are. Moreover, our MIC relations are valid in the metallicity range $-2.3 < [\text{Fe}/\text{H}] < 0.3$, and can be safely adopted in the range $-2.5 < [\text{Fe}/\text{H}] < 0.5$, taking into account the current uncertainties in spectroscopic abundances and in the metallicity scale. The metal-rich peak of our distribution is at the edge of the metallicity range covered by our MIC relations.

It is worth noticing that our photometric metallicity distribution for the RGs in the Baade’s window is also in fairly good agreement with the spectroscopic MDF obtained by the ARGOS survey for RGs in the Galactic bulge at latitude $b = -5^\circ$ (Ness et al. 2013a, see panel a) of their Fig. 11), with the spectroscopic MDF derived by Bensby et al. (2013) for a sample of 58 micro-lensed bulge dwarfs, and with the MDF obtained by

Uttenhaller et al. (2012) for a sample of ~ 400 RGs in the a region of the bulge centered at $(l, b) = (0^\circ, -10^\circ)$.

The above findings indicate that Strömgren–NIR photometry can provide solid constraints on the metallicity distribution not only of cluster RGs but also of field and halo bulge RGs. The key advantage of the current approach is that it can be applied to a large sample of field RGs located along different line of sight. The main drawback is that it requires accurate and deep photometry in at least three Strömgren bands (v, b, y) and at least one NIR band. However, accurate NIR photometry is now available for a significant fraction of the Galactic bulge (VISTA, Saito et al. 2012). An extensive use of the current approach is hampered by the fact that current wide field imager at 4–8m class telescopes are not equipped with high-quality Strömgren filters. It goes without saying that a medium–large Strömgren survey of the low-reddening regions of the Galactic bulge can have a substantial impact on our understanding of the bulge stellar populations. This means more quantitative constraints on the formation and evolution of the bulge and its chemical enrichment.

Acknowledgements. We thank Adriano Pietrinferni for his help with ZAHB models, and Elizabeth Fraser for helping us with the English. We acknowledge the referee for his/her pertinent comments and suggestions that helped us to improve the content and the readability of the manuscript. Support for this work has been provided by the IAC (grant 310394), and the Education and Science

Ministry of Spain (grants AYA2007-3E3506, and AYA2010-16717). This work was partially supported by PRIN INAF 2011 “Tracing the formation and evolution of the Galactic halo with VST” (PI: M. Marconi) and by PRIN-MIUR (2010LY5N2T) “Chemical and dynamical evolution of the Milky Way and Local Group galaxies” (PI: F. Matteucci). FM is thankful for the financial support from FONDECYT for project 3140177 and from the Chilean BASAL Centro de Excelencia en Astrofísica y Tecnologías Afines (CATA) grant PFB-06/2007. APM acknowledges the financial support from the Australian Research Council through Discovery Project grant DP120100475.

References

- Anthony-Twarog, B. J., & Twarog, B. A. 1994, *AJ*, 107, 1577 (ATT94)
- Anthony-Twarog, B.J., & Twarog, B.A. 1998, *AJ*, 116, 1922 (ATT98)
- Babusiaux, C., Gómez, A., Hill, V., Royer, F., Zoccali, M., Arenou, F., Fux, R., et al., 2010, *A&A*, 519, 77
- Bellman, S., Briley, M. M., Smith, G. H., Claver, C. F. 2001, *PASP*, 113, 326
- Bensby, T., Adén, D., Meléndez, J., Gould, A., Feltzing, S., Asplund, M., Johnson, J. A., et al., 2011, *A&A*, 533, A134
- Bensby, T., Yee, J. C., Feltzing, S., Johnson, J. A., Gould, A., Cohen, J. G., Asplund, M., et al., 2013, *A&A*, 549, 147
- Bertelli, G., Bressan, A., Chiosi, C., Fagotto, F., Nasi, E. 1994, *A&AS*, 106, 275
- Bond, H. E. 1970, *ApJS*, 22, 117
- Bono, G., Stetson, P. B., VandenBerg, D. A., Calamida, A., Dall’Ora, M., Iannicola, G., Amico, P., et al., 2010, *ApJ*, 708, L74
- Brasseur, C. M., Stetson, P. B., VandenBerg, D. A., Casagrande, L., Bono, G., Dall’Ora, M. 2010, *AJ*, 140, 1672
- Calamida, A., et al. 2005, *ApJ*, 634, L69
- Calamida, A., et al. 2007, *ApJ*, 670, 400 (CA07)
- Calamida, A., et al. 2009, *ApJ*, 706, 1277
- Calamida, A., et al. 2011, *ApJ*, 742, L28
- Calamida, A., et al. 2012, *A&A*, 544, 152
- Carbon, D. F., et al. 1982, *ApJS*, 49, 207
- Cardelli, J. A., Clayton, G. C., & Mathis, J. S. 1989, *ApJ*, 345, 245
- Carpenter, J. M. 2001, *AJ*, 121, 2851
- Carretta, E., Cohen, J. G., Gratton, R., Bradford, B. B. 2001, *AJ*, 122, 1469
- Carretta, E., Gratton, R., Bragaglia, A., Bonifacio, P., Pasquini, L. 2004, *A&A*, 416, 925
- Carretta, E., Bragaglia, A., Gratton, R., D’Orazi, V., Lucatello, S. 2009, *A&A*, 508, 695
- Castelli, F., & Kurucz, R. L. 1994, *A&A*, 281, 817
- Castelli, F., & Kurucz, R. L. 2006, *A&A*, 454, 333
- Catelan, M., Minniti, D., Lucas, P. W., et al. 2011, in *RR Lyrae Stars, Metal-Poor Stars, and the Galaxy*, ed. A. McWilliam, 145
- Chené, A. N., Borissova, J., Clarke, J. R. A., et al., 2012, *A&A*, 545, 54
- Coppola, G., Stetson, P. B., Marconi, M., Bono, G., Ripepi, V., Fabrizio, M., Dall’Ora, M., Musella, I., Buonanno, R., Ferraro, I., Fiorentino, G., Iannicola, G., Monelli, M., Nonino, M., Pulone, L., Thévenin, F., Walker, A. R. 2013, *ApJ*, 775, 6
- Crawford, D.L. 1975, *AJ*, 80, 955
- Cutri, R. M., Skrutskie, M. F., van Dyk, S., et al. 2003, “The IRSA 2MASS All-Sky Point Source Catalog, NASA/IPAC Infrared Science Archive, <http://irsa.ipac.caltech.edu/applications/Gator/>
- Dékány, I., Minniti, D., Catelan, M., Zoccali, M., Saito, R. K., Hempel, M., Gonzalez, O. A. 2013, *ApJ*, 776, 19
- Dell’Omodarme, M., Valle, G., Degl’Innocenti, S., & Prada Moroni, P. G. 2012, *A&A*, 540, 26
- Di Cecco, A., Becucci, R., Bono, G., Monelli, M., Stetson, P. B., Degl’Innocenti, S., Prada Moroni, P. G., et al., 2010, *PASP*, 122, 991
- Emerson, J., & Sutherland, W. 2010, *The Messenger*, 139, 2
- Faria, D., Feltzing, S., Lundstrom, I., Gilmore, G., Wahlgren, G.M., Ardeberg, A., Linde, P. 2007, *A&A*, 465, 357
- Feltzing, S., & Gilmore, G. 2000, *A&A*, 355, 949
- Feltzing, S., & Johnson, R. A. 2002, *A&A*, 385, 67
- Ferraro, F. R., Montegriffo, P., Origlia, L., Fusi Pecci, F. 2000, *AJ*, 119, 128
- Fiorentino, G., Stetson, P. B., Monelli, M., Bono, G., Bernard, E. J., Pietrinfermi, A. 2012, *ApJ*, 759, L12
- Francois, P. 1986, *A&A*, 160, 264
- Freeman, K., Ness, M., Wylie-de-Boer, E., Athanassoula, E., Bland-Hawthorn, J., Asplund, M., Lewis, G., et al., 2013, *MNRAS*, 428, 3660
- Fulbright, J.P. 2000, *AJ*, 120, 184
- Gonzalez, O. A., Rejkuba, M., Zoccali, M., Hill, V., Battaglia, G., Babusiaux, C., Minniti, D., Alves-Brito, A., Renzini, A., Gomez, A., Ortolani, S. 2011, *A&A*, 530, 54
- Gratton, R., Sneden, C., Carretta, E. 2004, *ARA&A*, 42, 385
- Grundahl, F., VandenBerg, D. A., Bell, R. A., Andersen, M. I., Stetson, P. B. 2000, *AJ*, 120, 1884
- Grundahl, F., Stetson, P. B., Andersen, M.I. 2002, *A&A*, 395, 481
- Gustafsson B., Edvardsson B., Eriksson K., Jürgensen U.G., Nordlund C., Plez B. 2008, *A&A*, 486, 951
- Harris, W.E. 2003, *Catalog of Parameters for Milky Way Globular Clusters: The Database* Hamilton: McMaster Univ., <http://physun.physics.mcmaster.ca/~harris/mwgc.dat>
- Hauschildt, P. H., Allard, F., & Baron, E. 1999a, *ApJ*, 512, 377
- Hauschildt, P. H., Allard, F., Ferguson, J., Baron, E., & Alexander, D. 1999b, *ApJ*, 525, 871
- Haywood, M. 2001, *MNRAS*, 325, 1365
- Haywood, M. 2002, *MNRAS*, 337, 151
- Heasley, J. N., Janes, K. A., Zinn, R., Demarque, P., Da Costa, G. S., Christian, C. A. 2000, *AJ*, 120, 879
- Hilker, M. 2000, *A&A*, 355, 994
- Hill, V., Lecœur, A., Gómez, A., Zoccali, M., 2011, *A&A*, 534, 80
- Irwin, M. J., Lewis, J., Hodgkin, S., et al., 2004, in *Society of Photo-Optical Instrumentation Engineers (SPIE) Conference Series*, Vol. 5493, ed. P. J. Quinn, A. Bridger, 411 422
- Kraft, R. P. 1994, *PASP*, 106, 553
- Kraft, R. P., Ivans, I. I. 2003, *PASP*, 115, 143
- Lagioia, E. P., Milone, A. P., Stetson, P. B., Bono, G., Prada Moroni, P. G., Dall’Ora, M., Aparicio, A., Buonanno, R., Calamida, A., Ferraro, I., Gilmozzi, R., Iannicola, G., Matsunaga, N., Monelli, M., Walker, A. 2014, *ApJ*, 782, 50(LA14)
- Langer, G. E., Kraft, R. P., Carbon, D. F., Friel, E., Oke, J. B. 1986, *PASP*, 98, 473
- Mauro, F., Moni Bidin, C., Geisler, D., Saviane, I., Da Costa, G. S., Gormaz-Matamala, A. C., Vasquez, S., Chen, A.-N., Cohen, R., Dias, B. 2014, *A&A*, accepted, arXiv1401.0014M
- Mauro, F., Moni Bidin, C., Chené, A.-N., Geisler, D., Alonso-Garcia, J., Borissova, J., Carraro, G. 2013, *RevMxAA*, 49, 189
- Milone, A. P., Bedin, L. R., Piotto, G., Anderson, J., King, I. R., Sarajedini, A., Dotter, A., Chaboyer, B., et al., 2008, *ApJ*, 673, 241
- Milone, A. P., Piotto, G., Bedin, L. R., King, I. R., Anderson, J., Marino, A. F., Bellini, A., et al., 2012, *ApJ*, 744, 58
- Minniti, D., Lucas, P. W., Emerson, J. P., et al., 2010, *New Astronomy*, 15, 433
- Momany, Y., Ortolani, S., Held, E. V., Barbuy, B., Bica, E., Renzini, A., Bedin, L. R., Rich, R. M., Marconi, G. 2003, *A&A*, 402, 607
- Moni Bidin, C., Mauro, F., Geisler, D., et al., 2011, *A&A*, 535, 33
- Ness, M., Freeman, K., Athanassoula, E., Wylie-de-Boer, E., Bland-Hawthorn, J., Asplund, M., Lewis, G. F., Yong, D., Lane, R. R., Kiss, L. L. 2013, *MNRAS*, 430, 836
- Nissen, P. E. 1981, *A&A*, 97, 145
- Nissen, P. E. 1988, *A&A*, 199, 146
- Nissen, P.E., Schuster, W. J. 1991, *A&A*, 251, 457
- Nissen, P.E. 1994, *RMxAA*, 29, 129
- Olsen, E. H. 1983, *A&AS*, 54, 55
- Olsen, E. H. 1984, *A&AS*, 57, 443
- Olsen, E. H. 1988, *A&A*, 189, 173
- Olsen, E. H. 1993, *A&AS*, 102, 89
- Origlia, L., Valenti, E., Rich, R. M. *MNRAS*, 356, 1276
- Pietrinfermi, A., Cassisi, S., Salaris, M., Castelli, F. 2004, *ApJ*, 612, 168
- Pietrinfermi, A., Cassisi, S., Salaris, M., Castelli, F. 2006, *ApJ*, 642, 697 (PI06)
- Pietrinfermi, A., Cassisi, S., Salaris, M., Percival, S., Ferguson, J. W. 2009, *ApJ*, 697, 275
- Pilachowski, C. A., Bothun, G. D., Olszewski, E. W., Odell, A. 1983, *ApJ*, 273, 187
- Richter, P., Hilker, M., & Richtler, T. 1999, *A&A*, 350, 476
- Rutledge, G.A., et al. 1997, *PASP*, 109, 907
- Saito, R. K., Zoccali, M., McWilliam, A. M., Minniti, D., Gonzalez, O. A., Hill, V. 2011, *AJ*, 142, 76
- Saito, R., Hempel, M., Minniti, D., Lucas, P. W., Rejkuba, M., Toledo, I., Gonzalez, O. A., et al., 2012, *A&A*, 537, 107
- Salasnich, B., Girardi, L., Weiss, A., Chiosi, C. 2000, *A&A*, 361, 1023
- Salaris, M., Chieffi, A., & Straniero, O. 1993, *ApJ*, 414, 580
- Saviane, I., Da Costa, G. S., Held, E. V., Sommariva, V., Gullieuszk, M., Barbuy, B., Ortolani, S. *A&A*, 540, 27(SA12)
- Sbordone, L., Salaris, M., Weiss, A., Cassisi, S. 2011, *A&A*, 534, A9
- Schlegel, D. J., Finkbeiner, D. P., & Davis, M. 1998, *ApJ*, 500, 525
- Schuster, W. J., Nissen, P. E. 1988, *A&AS*, 221, 65
- Schuster, W. J., Nissen, P.E. 1989, *A&AS*, 73, 225 (SN89)
- Sneden, C., Kraft, R. P., Prosser, C. F., Langer, G. E. 1991, *AJ*, 102, 2001
- Skrutskie, M. F., Cutri, R. M., Stiening, R., et al., 2006, *AJ*, 131, 1163
- Sousa, S. G., Santos, N. C., Mayor, M., Udry, S., Casagrande, L., Israelian, G., Pepe, F., Quélou, D., Monteiro, M. J. 2008, *A&A*, 487, 373
- Stetson, P. B. 1987, *PASP*, 99, 191
- Stetson, P. B. 1990, *PASP*, 102, 932
- Stetson, P. B. 1991, *AJ*, 102, 589

- Stetson, P. B. 1993, IAU Colloq. 136: Stellar Photometry - Current Techniques and Future Developments, 291
- Stetson, P. B. 1994, PASP, 106, 250
- Stetson, P. B., Bruntt, H., & Grundahl, F. 2003, PASP, 115, 413
- Strömgren, B. 1964, ApNr, 9, 333
- Strömgren, B. 1966, Ann.Rev. A&A, 4, 433
- Thèvenin, F., & Idiart, T. P. 1999, ApJ, 521, 753
- Utenthaler, S., Schultheis, M., Nataf, D. M., Robin, A. C., Lebzelter, T., Chen, B. 2012, A&A, 556, 38
- Valenti, J. A., Fischer, D. A. 2005, ApJS, 159, 141
- Valenti, E., Ferraro, F. R., Origlia, L. 2004, MNRAS, 351, 1204
- Valenti, E., Origlia, L., Rich, R. M. 2011, MNRAS, 414, 2690
- van Loon, Jacco Th., Gilmore, G. F., Omont, A., Blommaert, J. A. D. L., Glass, I. S., Messineo, M., Schuller, F., Schultheis, M., Yamamura, I., Zhao, H. S. 2003, MNRAS, 338, 857
- Vásquez, S., Zoccali, M., Hill, V., Renzini, A., González, O. A., Gardner, E., Debattista, V. P., Robin, A. C., Rejkuba, M., Baffico, M., Monelli, M., Motta, V., Minniti, D. 2013, A&A, 555, 91
- Zinn, R., & West, M. J. 1984, ApJS, 55, 45
- Zoccali, M., Barbuy, B., Hill, V., Ortolani, S., Greggio, L., Saviane, I., Cassisi, S., Rejkuba, M., Barbuy, B., Rich, R. M., Bica, E. 2003, A&A, 399, 931
- Zoccali, M., Renzini, A., Ortolani, S., Renzini, A., Bica, E., Momamy, Y., Pasquini, L., Minniti, D., Rich, R. M. 2004, A&A, 423, 507 (ZO04)
- Zoccali, M., Lecureur, A., Barbuy, B., Hill, V., Renzini, A., Minniti, D., Momamy, Y. 2006, A&A, 457, L1
- Zoccali, M., Hill, V., Lecureur, A., Barbuy, B., Renzini, A., Minniti, D., Gómez, A., Ortolani, S. 2008, A&A, 486, 177(ZO08)